POLITECNICO DI MILANO
School of Industrial and Information Engineering

Master of Science in Physics Engineering

Applications of a Fourier-Transform Hyperspectral Camera to Vertical Farming

Supervisor: Prof. Dario Polli
Co-supervisor: Antonio Perri
Co-supervisor: Fabrizio Preda

Candidate:
Marta Provera
Matr. 928566

Academic Year 2020-2021

Abstract

Hyperspectral imaging (HSI) technology aims at recovering the full spectra of the light coming from of each point of a 2-dimensional image. The analysis of the data provided by this technique enables the user to retrieve physicochemical properties of the imaged object. Due to its characteristics of non-invasivity, reliability and flexibility, hyperspectral imaging is nowadays being applied in a continuously growing number of fields, both in the academic and industrial world. In particular the present work will concentrate on the applications of HSI in the food and agriculture sector. The attention that nowadays customers put on the quality of food they purchase, requires the companies a constant control over their products. Hyperspectral imaging technology offers them a fast and reliable mean to monitor the condition of the whole production chain, enabling the producers to fulfill customer's standards. HSI has been implemented using various technologies. In particular, in the present work all the analysis have been carried out with a hyperspectral camera produced by NIREOS: a spinoff company of the Politecnico di Milano. The technology of the HERA Iperspettrale camera is based on Fourier-Transform spectroscopy, exploiting a patented ultra-stable common-path birefringent interferometer. The main focus of this thesis is the employment of the HERA hyperspectral camera to study the spectral signatures that characterize the growing and senescence of leafy vegetables grown in a vertical farm. Fundamental nutrients inside the plants indeed, like chlorophylls and phenols, have specific absorption regions in the VIS-NIR and information on their concentration can be retrieved by the analysis of the sample's spectra. The technology of the HERA Iperspettrale enables also to perform measurements of the fluorescence spectrum of the leaves, from which it is possible to extract data on the photosynthetic potential of the plant. Two projects will be presented throughout the work. The first one concentrates on the spectral features that indicate senescence in leafy vegetables in three different conservation techniques. The way in which the samples are stored will greatly influence their degradation process, leading to

different detectable signs of senescence in the spectra. The second study instead tries to analyze the effect of biostimulants on leafy vegetables in their growth and senescence process. The effect of these compounds is more difficult to distinguish, rather the study will provide further information on the evolution of the plant's spectra during their growth or degradation.

Keywords: Hyperspectral Imaging; Fourier-Transform Spectroscopy; Absorption spectrum; Reflectance spectrum; Fluorescence spectrum; Agriculture; Food

Estratto

La tecnologia dell'Imaging Iperspettrale volge alla ricostruzione dell'intero spettro della luce proveniente da ogni punto di un'immagine bidimensionale. L'analisi dei dati forniti da questa tecnica ci permette dunque di recuperare proprietà fisico-chimiche dell'oggetto rappresentato. Grazie alle sue caratteristiche di non-invasività, affidabilità e flessibilità, l'imaging iperspettrale oggi è applicato in un crescente numero di campi, sia nel mondo accademico che industriale. Questo elaborato in particolare si concentra sull'applicazione dell'imaging iperspettrale nel campo dell'agricoltura e degli alimenti. L'attenzione che oggi i consumatori mettono nella qualità e nella scelta del cibo che acquistano, richiede alle compagnie un controllo costante dei loro prodotti. La tecnologia dell'imaging iperspettrale offre loro un mezzo veloce ed affidabile per monitorare le condizioni di tutta la catena di produzione, permettendogli di soddisfare le aspettative dei consumatori. L'imaging iperspettrale è stato implementato con varie tecnologie, in particolare in questo lavoro tutte le analisi sono state svolte con una camera iperspettrale prodotta da NIREOS: una compagnia spinoff del Politecnico di Milano. La tecnologia della HERA Iperspettrale è basata sulla spettroscopia a Trasformata di Fourier impiegando un interferometro birifrangente common-path ultra stabile brevettato. Lo scopo principale di questo elaborato è l'utilizzo della HERA Iperspettrale per studiare le caratteristiche dello spettro che indicano segni di crescita e senescenza di verdure a foglia coltivate con agricoltura verticale. Nutrienti fondamentali delle piante, come la clorofilla ed i fenoli hanno specifiche finestre di assorbimento nella regione del VIS-NIR e informazioni riguardanti la loro concentrazione possono essere ricavate dall'analisi dello spettro dei campioni. La tecnologia della HERA Iperspettrale permette inoltre di effettuare misure dello spettro di fluorescenza delle foglie, dal quale è possibile estrarre dati sulla capacità fotosintetica della pianta. Due progetti verranno presentati nell'elaborato. Il primo si concentra sulle caratteristiche spettrali che indicano segni di senescenza nei vegetali a foglia in tre diverse condizioni di conservazione. Si vedrà che il modo in cui i campioni sono preservati influenza in modo rilevante il loro processo di degradazione, portando a diversi segni di invecchiamento osservabili negli spettri. Il secondo studio invece si propone di analizzare gli effetti dell'applicazione di biostimolanti ai vegetali a foglia sulla loro crescita ed invecchiamento. L'effetto di questi composti è più difficile da distinguere,

piuttosto lo studio darà ulteriori informazioni sull'evoluzione degli spettri delle piante durante la loro crescita o degradazione.

Parole Chiave: Imaging Iperspettrale; Spettroscopia a Trasformata di Fourier; Spettro di assorbimento; Spettro di riflessione; Spettro di florescenza; Agricoltura; Alimenti

Contents

List of Figures

Chapter 1

Introduction

Imaging is a powerful tool to remotely analyze samples in a non-destructive and reliable way. Among all the technologies available for this purpose, Hyperspectral Imaging (HSI) is one of the most effective. HSI systems are indeed able to retrieve the full spectra of the light coming from each point of the imaged object. In 2018 NIREOS s.r.l., a spinoff company of the Politecnico di Milano, developed the HERA Iperspettrale: a hyperspectral camera based on Fourier-Transform spectroscopy. The present work aims at investigating the possibilities of application of the HERA Iperspettrale in food and agriculture. The employment of innovative technology in this sector is nowadays gaining importance in the development of quality-checking automated techniques. Furthermore, recent studies demonstrated the possibilities of retrieving physicochemical properties of leafy vegetables from the analysis of their spectra [1],[2],[3],[4]. The HERA Iperspettrale has been employed in this work to monitor the growth and senescence of leafy vegetables in various conditions and investigate whether wellness or degradation signs are distinguishable in the spectra of the samples. The research projects have been carried out as a collaboration between NIREOS and Agricola Moderna: a vertical farm based in Milan. The original contribution of this thesis consists in the completion of the aforementioned project, from the measurement campaigns to the development of algorithms to visualize and analyze the collected hyperspectral data. In order to understand the functioning of the HERA Iperspettrale and the managing of the hyperspectral data, some preliminary measurements on different kind of samples have also been carried out.

1.1 Structure

In this section a brief outline of the subject matters of the next chapters is presented:

- *Chapter 2*: the fundamental concepts of hyperspectral imaging will be outlined

together with the various methodologies to implement it. In particular, the technology underneath the HERA Iperspettrale will be deepened.

- *Chapter 3*: how to manage the hyperspectral data will be the topic at the center of this chapter. The most important algorithms employed later in the work will be presented.

- *Chapter 4*: the whole possibilities of application of the HSI technology will be explained throughout this chapter. Finally the employment of these systems to the food and agriculture field will be highlighted.

- *Chapter* 5: the results of the application of the HERA Iperspettrale to study growth and senescence of leafy vegetables will be shown in this chapter.

- *Chapter 6*: will present the main conclusions derived from the measurement analysis of the previous chapter. Finally some insights on future works and developments will be examined.

Chapter 2

Hyperspectral imaging: an overview

In the next sections the basic concepts of Hyperspectral Imaging will be introduced. Moreover, the most common technologies applied to this field are going to be reviewed and finally the device at the center of the present work will be described: the HERA Iperspettrale hyperspectral camera. The great advantages and possibilities of the camera will be clear after the analysis of the theoretical basis of Fourier-Transform spectroscopy and its technological implementation with the patented common-path birefringent interferometer TWINS.

2.1 Introduction to Hyperspectral Imaging

Hyperspectral imaging (HSI) is nowadays a powerful tool to be applied in the most various contexts, ranging from medical and biological imaging to conservation of cultural heritage and agriculture. The HSI technology aims at measuring the spectrum of the light coming from each point of the scene under analysis [5].

Common RGB cameras exploit a mechanism similar to the one of the human eye, which has three kinds of cone cells that sense light, having peaks of sensitivity in the red, green and blue spectral region. This kind of technology reconstruct images by combining the amount of red, green and blue for each pixel of the scene of interest, indeed their combination can give rise to any color [6].

More refined approaches are able to retrieve a bigger amount of spectral information from the image, enabling, other than the color analysis, to acquire data on the chemical composition of the scene or recover physical quantities of the sample. For example, a first

improvement to the RGB technology is *multispectral imaging* where, for each pixel of the image, more than three bands (typically around 10 to 15) are acquired. By increasing the number of bands up to almost a continuum it is possible to reconstruct the spectrum of the light coming from each pixel with fine spectral resolution, not only in the visible range but also in the infrared [5]. This approach is at the core of the Hyperspectral Imaging technology.

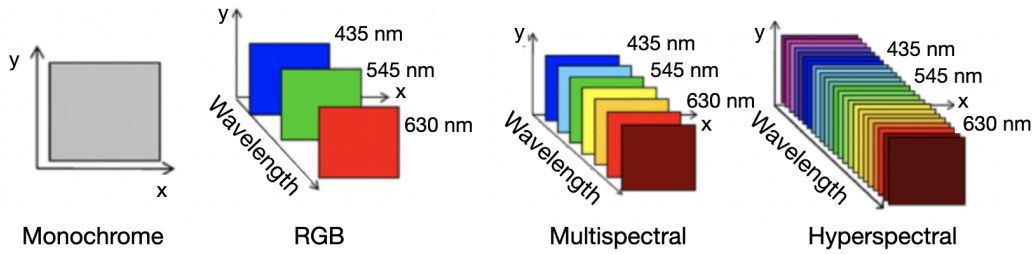

Figure 2.1: Display of the acquisition bands for the mentioned imaging techniques.

2.2 The hyperspectral cube

The information that is retrieved from a hyperspectral measure is organized in the *hyperspectral cube*: a (x,y,λ) matrix where for each pixel (x,y) of the scene of interest, the values in the z direction represent the intensities for the k spectral bands (Figure 2.2).

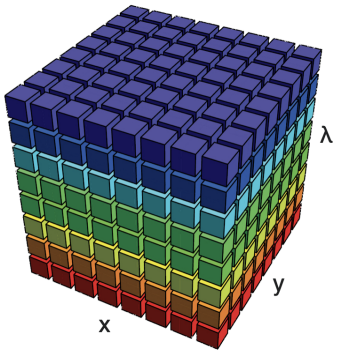

Figure 2.2: Graphical representation of the hyperspectral cube.

These cubes contain a massive amount of information. In order to retrieve quantitative parameters, relevant for the physical and chemical analysis of the sample, these data have to be analyzed by means of numerical methods and specific algorithms, that will

be presented in Chapter 3. Also, this extensive amount of data enables the application of machine learning techniques, supervised or unsupervised, to the hyperspectral cube, which can be used to perform both clustering into different components of the image and classification processes. These methods could be very useful in detecting finer patterns and differences in the spectra, not visible with simpler numerical methods.

2.3 HSI technologies

Hyperspectral imaging has been implemented with various technologies, each one with its advantages and drawbacks. In this section the most common techniques will be briefly described.

Every HSI setup has to be composed by three main elements:

- **Light source**: different options are available depending on the application. A broadband source, such as a halogen lamp, can be used for example in order to cover a large portion of the spectrum. Otherwise many LEDs, combined if needed with other halogen lamps, can be employed to cover an even wider range of wavelengths: from the visible range to the infrared one. On the other hand, some applications, such as remote sensing, simply exploit ambient light as a source.
- **Optics**: depending on the kind of acquisition required, different optical elements are inserted in the acquisition chain. In some technologies, optical filters are exploited to select subsequent wavelengths and cover the whole spectrum. In other methods instead, a dispersive element, such as a prism or grating, is used to separate the different components of the spectrum.
- **Detection system**: different kind of detectors enable the analysis of different portions of the spectrum of the light coming from the sample.

Practically the measurement consists in collecting the diffuse reflectance coming from the illuminated sample through suitable optical elements. By combining different sources, optical elements and detectors, a variety of HSI setup systems can be developed [6]. The most important configurations are presented in the next sections.

2.3.1 Point-scan or whisk-broom HSI

This configuration (Figure 2.3) acquires the whole spectrum for a single pixel of the image. Clearly the sample or the source have to be moved to cover the whole matrix of the pixels. This system provides very stable high resolution spectra, however the

repositioning of the sample is quite time consuming and limits the acquisition time: that is the main drawback of this approach.

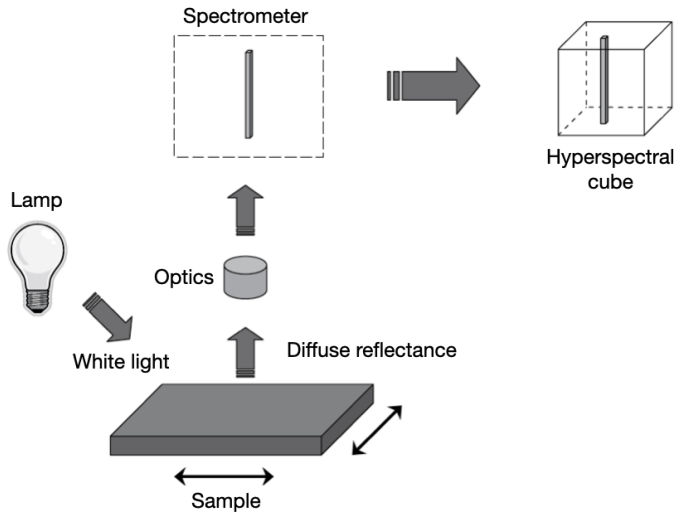

Figure 2.3: Point-scan measurement setup.

2.3.2 Line-scan or push-broom HSI

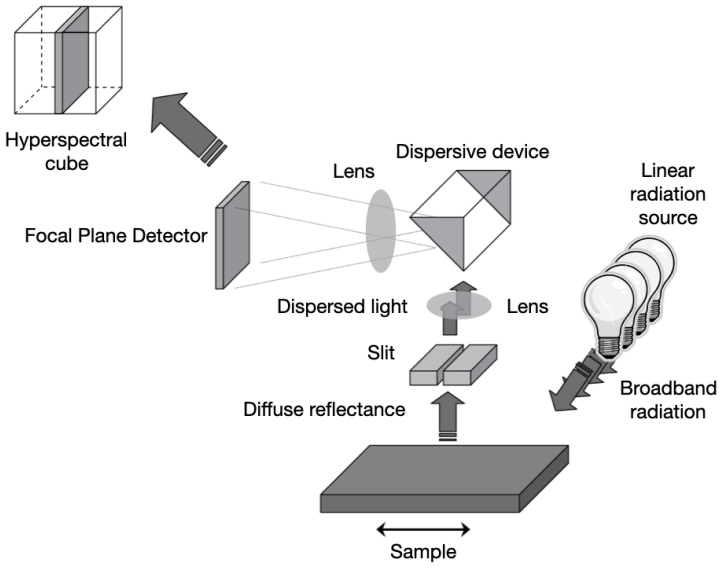

Figure 2.4: Line-scan measurement setup.

Acquisition time is improved in this configuration, indeed light coming from a line of the sample is detected through a slit placed before the detector as shown in Figure 2.4. Finally, a dispersive element separates the wavelengths, and their relative intensity is measured at the detector that is placed perpendicularly to the surface of the sample. Also in this case either the sample or the source have to be moved in order to acquire a plane of the hyperspectral cube at a time. This technique is widely used in industrial and commercial applications, however, it implies high losses due to the presence of the slit which limits the acquisition time.

2.3.3 Focal plane scanning imaging

In this configuration a set of bandpass filters is used to select the wavelengths and acquire the intensities relative to all the 2D-matrix of pixels. Therefore, this method requires a change of the filter for the acquisition of each plane of the hyperspectral cube, as represented in Figure 2.5, while the position of the sample remains fixed. Selection of wavelength can be implemented by using interference filters, like liquid crystal tunable filters (LCTFs) or cousto-optic tunable filters (AOTFs). The change of filters in this case can be implemented electronically. It is easy to understand that the image acquisition time is quite lengthy for this configuration.

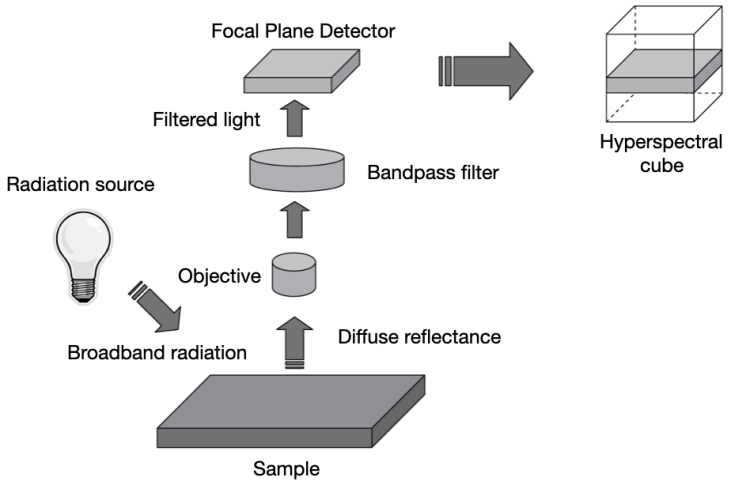

Figure 2.5: Focal plane measurement setup.

2.3.4 Snapshot HSI

Oppositely to the scanning techniques described previously (see Figure 2.6(a)), which acquire only a portion of the data cube at a time, snapshot configurations enable one

to obtain the whole hyperspectral cube with a single measurement (Figure 2.6(b)) [7]. These methods are therefore characterized by a short acquisition time compared to the previously presented systems.

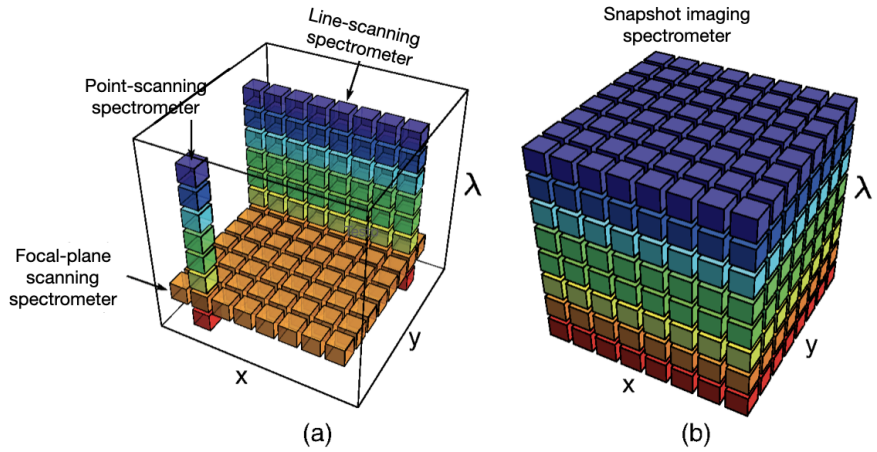

Figure 2.6: Hyperpsectral cube acquisition for (a) scanning techniques (b) snapshot techniques.

Snapshot techniques can be classified in two categories, based on their light-collection capacity: "full-throughput" and "throughput-division". Throughput-division techniques lose some optical-throughput due to the presence of filters in their setup. These technologies have a similar functioning to the one of standard RGB cameras but more filters are required to acquire a bigger number of bands. Figure 2.7(a) shows a Division of APerture (DoAP) system. In DoAPs the detector is composed of an array of mini-cameras each with its own spectral filter. This devices have the major drawback of acquiring a number of bands which is limited by the number of filters on the detector. A different throughput-division technology is represented Figure 2.7(b): the Division of Focal Plane (DoFP). In this case a filter is placed over each individual pixel [8]. This acquisition method limits the spatial resolution since pixels are employed to spectrally resolve light of the imaged object.
Full-throughput snapshot techniques are technologically more complex, however they do not employ filters in their configuration and guarantee a high efficiency and high optical throughput. The adoption of these devices has become possible thanks to the recent technological advances in fabrication of very small optical elements and systems with a large amount of sensing elements.

Finally, in the next section, Fourier-Transform (FT) spectroscopy will be analyzed in detail. This technology is indeed at the core of the HERA Iperspettrale hyperspectral

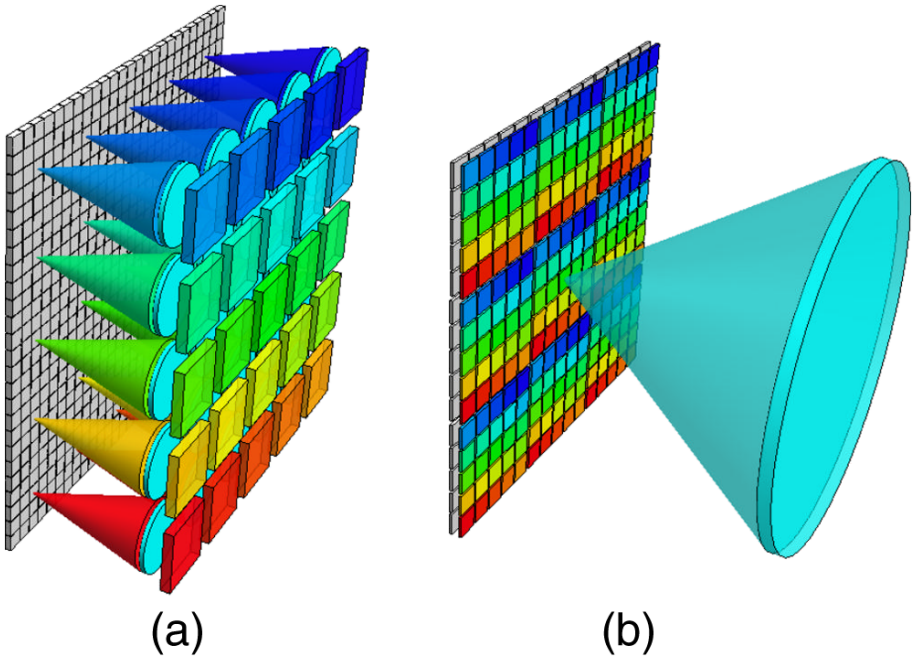

Figure 2.7: Throughput-division snapshot techniques: (a) Division of APerture (DoAP) (b) Division of Focal Plane (DoFP).

camera.

2.4 The HERA Iperspettrale

Figure 2.8: The HERA Iperspettrale hyperspectral camera.

All the hyperspectral analysis performed in this work were carried out with the HERA Iperspettrale hyperspectral camera, produced by NIREOS s.r.l. [1]: a spinoff company from Politecnico di Milano. This device employs FT spectroscopy in order to obtain hyperspectral measures; the basic principles of this technique will be deepened in the next section. Finally, the functioning of the common-path interferometer at the basis of the HERA technology will be presented.

2.4.1 Fourier-Transform spectroscopy

Optical spectroscopy can be divided in two broad categories: frequency domain (presented in the previous sections) and time domain. An example of the time domain approach is represented by Fourier-Transform spectroscopy. This technique combines a monochrome imaging sensor with an interferometer to retrieve the continuous spectrum of a scene from the interferogram. To obtain the interferogram, the light coming from the sample of interest is split in two collinear delayed replicas and their interference

[1] More information is available on NIREOS website: https://www.nireos.com/hera/

pattern is measured as a function of the relative delay [9]. For a fixed time delay τ, the interferogram $I(\tau)$ is given by the the interference of $E(t)$ and its delayed replica $E(t+\tau)$:

$$I(\tau) = \int |E(t) + E(t+\tau)|^2 dt \tag{2.1}$$

$$I(\tau) = 2\int |E(t)|^2 dt + \int E(t)E^*(t+\tau)dt + c.c. \tag{2.2}$$

Only the second oscillating AC term in Equation 2.2 is relevant for the spectrum of the electric field while the first component is a constant DC term that can be neglected. Finally the spectrum can be obtained performing the Fourier-Transform of the interferogram $I(\tau)$, as stated by the Wiener-Khinchin theorem [10]:

$$F(I(\tau)) = \tilde{I}(\omega) = \tilde{E}^*(\omega)\tilde{E}(\omega) + c.c = 2|\tilde{E}(\omega)|^2 = 2\tilde{I}(\omega) \tag{2.3}$$

The advantages of obtaining the continuous spectrum of light from the FT of the interferogram are numerous and already well-known [11]:

- *Fellgett's advantage*: all the wavelengths in this configuration are measured simultaneously, leading to a higher number of photons at the detector and, consequently, a higher signal-to-noise ratio in the system where the main source of noise is the detector.
- *Jaquinot's advantage*: in FT systems, the absence of slits, which, as stated in the previous paragraph, cause losses, leads to a higher throughput.
- *Connes' advantage*: high wavelengths accuracy, indeed the device is calibrated through a laser beam.
- *Variable spectral resolution*: varying the maximum delay of the interferometer, it is possible to adjust at will the spectral resolution. This is done without affecting the throughput of the device.
- *Variable spatial resolution*: can be adjusted without affecting spectral resolution.

FT spectroscopy can be implemented either in a static or scanning approach [5]. In the first case, the interferometer has no moving parts and the sample is moved at each acquisition to obtain the interferogram along all the dimensions of the image. This method is most suitable for applications in industrial fields where the object is moving along a production line on a conveyor belt or in airborne remote sensing. Instead, in the case of stationary objects, the scanning approach is more convenient. In this second case there is no need to move the object relatively to the camera because the interferometer

is equipped with a moving element that is scanned to vary the delay of the replicas. The basic scheme of an interferometer adopted in the temporal approach is represented by the Michelson interferometer [9], displayed in Figure 2.9.

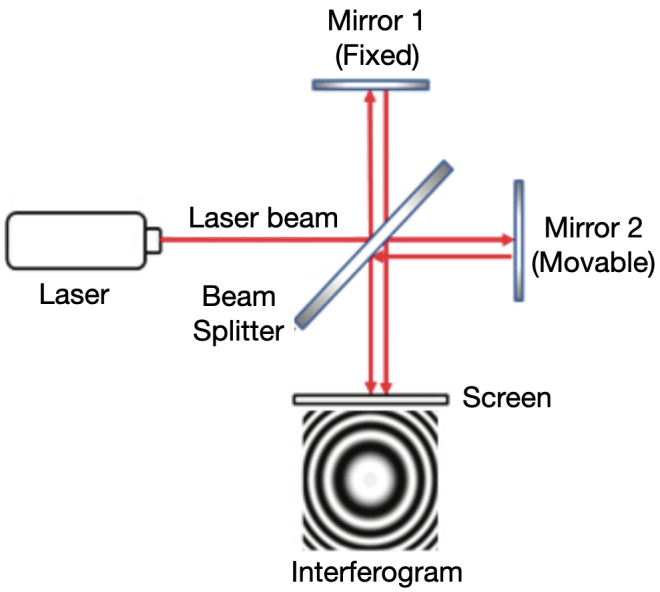

Figure 2.9: Scheme of the Michelson interferometer.

The beam coming from the sample is split in two replicas by a beam splitter which reflects half of the light towards a fixed high reflectance mirror; similarly, the transmitted light is directed to another mirror which can be moved to obtain the desired delay. The two replicas encounter again at the beam splitter after having covered a different optical path and their interference pattern is measured at the detector. However, HSI systems based on the Michelson or, similarly, Mach-Zehnder interferometer, where the beams take two different paths, are highly sensitive to vibrations and it is difficult to achieve the interferometric stability required to obtain high quality spectra. Indeed two essential conditions must be met by a FT-spectrometer:

- the relative delay between the two replicas must be controlled within a fraction of the optical cycle.
- for a given pixel, the bundle of rays giving the interferogram must have a high degree of coherence.

At the basis of the HERA Iperspettrale lays a Common-Path birefringent Interferometer [12]: the Translating-Wedge-Based Identical Pulses eNcoding System (TWINS) which is

also able to overcome the limitation due to vibrations. The TWINS technology will be presented in the next paragraph.

2.4.2 TWINS

The Translating-Wedge-Based Identical Pulses eNcoding System (TWINS) is a common-path birefringent interferometer developed by a collaboration of the Politecnico di Milano and the Centro Nazionale di Ricerca (CNR) [13]. Its scheme is represented in Figure 2.10. It is composed of two polarizers P1 and P2 and two birefringent blocks A and B made of α-barium borate ($\alpha - BBO$).

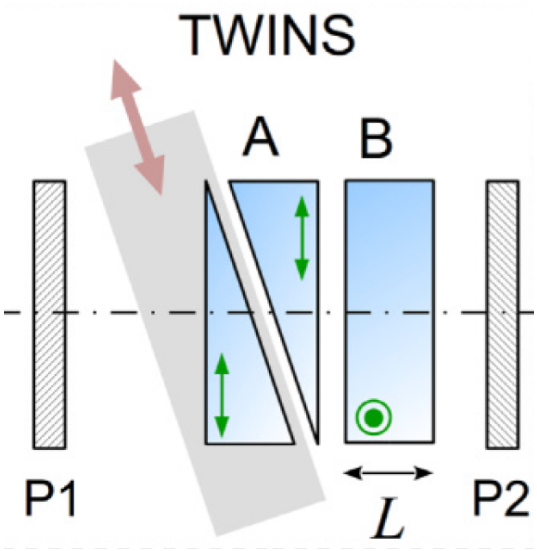

Figure 2.10: Scheme of the TWINS interferometer.

- P1 polarizes the incoming light at 45° with respect to the optical axes of A and B.
- Block A is shaped as two wedges with the same apex angle where one of them is mounted on a motorized translation stage in order to tune the relative thickness of this first block with respect to B. It enables the creation of two replicas of the incoming light which travel with perpendicular polarization along the two axis of the material with a delay τ that can be tuned by the movement of the wedge.
- Block B is a plate with fixed thickness that introduces therefore a fixed phase delay with opposite sign with respect to the one introduced by A since the two blocks have perpendicular optical axis (see green arrows in Figure 2.10).

- P2 projects again the two replicas on the same polarization, at 45° with respect to the blocks' axis and guarantees the interference of the two replicas at the detector.

It is clear that the technology underneath this device is able to meet both the demands presented in the previous section to obtain high quality spectra: control of the delay of the replicas and high coherence of the rays. Indeed, since the replicas travel along the same path, they are subjected in the same way to vibrations and the overall measurement will not be affected. Furthermore, the travelling replicas have small geometrical separation, leading to a high coherence of the bundle of rays and a strong interference[14].

The final scheme for the HERA Iperspettrale is presented in Figure 2.11 [15].

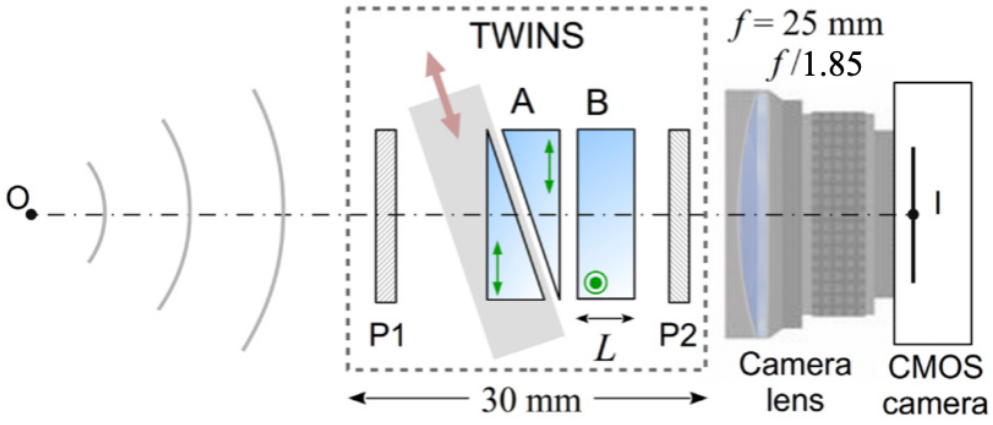

Figure 2.11: Scheme of the HERA Iperspettrale.

In the hyperspectral camera the TWINS interferometer is combined with a lens with focal length $f = 25$ mm and maximum aperture $f/1.85$ and finally a 1280×1024 monochrome silicon CMOS sensor. The overall angular field of view of the system is of 16°. The hyperspectral cube is obtained by acquiring multiple images at different position of the interferometer, obtaining for each pixel of the scene a broadband spectrum from the UV to the Near Infrared (NIR) region (400 nm - 1000 nm) [5].

2.4.3 Fluorescence spectroscopy

Thanks to its high sensitivity and high light throughput, combined to the fact that measurements are performed in a staring configuration, the HERA Iperspettrale is particularly suitable for measurements performed in low light conditions and can also provide

fluorescence measurements, unlike other hyperspectral cameras. In fluorescence measurements, as it will be presented later in the work, the sample is excited through a LED lamp and photons emitted by fluorescent substances in the specimen are recorded at the detector. In detection, to cut off the excitation light, a long-pass filter is applied. With this setup it is possible to recover the fluorescence spectra of every pixel of the image, starting from a hyperspectral cube that has the same characteristics of the one provided by standard measurements. However, fluorescence spectroscopy is particularly useful and can provide very interesting information in applications related to biological sciences. Fluorescence indeed is employed in cell identification, detection of nutrients and chemical components in plants (as we will deepen later) and many medical tests are based on this phenomenon [16].

Chapter 3

Hyperspectral data analysis

As previously noted, the data emerging from a hyperspectral measure provide an extensive amount of information which have to be analyzed and manipulated through numerical methods in order to retrieve relevant and understandable quantities. In the current chapter the most important algorithms which have been applied to the hyperspectral measurements will be briefly explained. All the corresponding code has been implemented using the MATLAB programming language and some simple lines of code are reported to better understand some concepts. More detailed algorithms are reported in the Appendix. Measurements performed with the HERA Iperspettrale provide a hyperspectral cube of dimensions $(1024 \times 1280 \times 120)$. Indeed for each pixel (x, y) the camera measures the intensities related to 120 bands.

3.1 Spectra analysis: absolute and reflectance spectrum

Recovering the spectrum of a pixel or a portion of the hyperspectral image requires some kind of manipulation of the hyperspectral cube. To retrieve the spectrum of a single pixel, the corresponding portion of the 3-D data cube should be selected, the procedure is performed in MATLAB simply as:

$$spectrum = hyperspectralCube(x, y, :) \tag{3.1}$$

selecting all the bands corresponding to the desired pixel (x,y) in the image. In many cases, in order to infer more significant information on the sample, the spectra that will be taken into consideration in the present work will be referred to an area rather than a single pixel of the image. These spectra are calculated by manually selecting an area of the image and mediating over the single-pixel spectra.

Also, it is important to consider that the intensity of the light coming from a real sample is subjected to its relative position and orientation with respect to the camera and the light source. The object might present portions with different orientation that are illuminated in a non-homogeneous way. To obtain relevant and meaningful quantities and spectra that are comparable with each other, the measurements have to be normalized. Ideally, this should be done by taking the absolute data cube of the specimen and dividing it by the hyperspectral cube relative to the light coming from a lambertian surface which has the same shape and orientation of the sample. A lambertian surface is an ideal diffusive surface which reflects the incoming light in the same way in all directions regardless of the observation angle. It is therefore a surface with isotropic luminance. In the present work we will mainly refer to normalized quantities which are called *reflectance spectra*. Later on also the experimental method to measure a lambertian and a reflectance spectrum will be presented. Figure 3.1 shows the absolute and reflectance spectrum relative to the selected area for a sample composed of different species of lettuce.

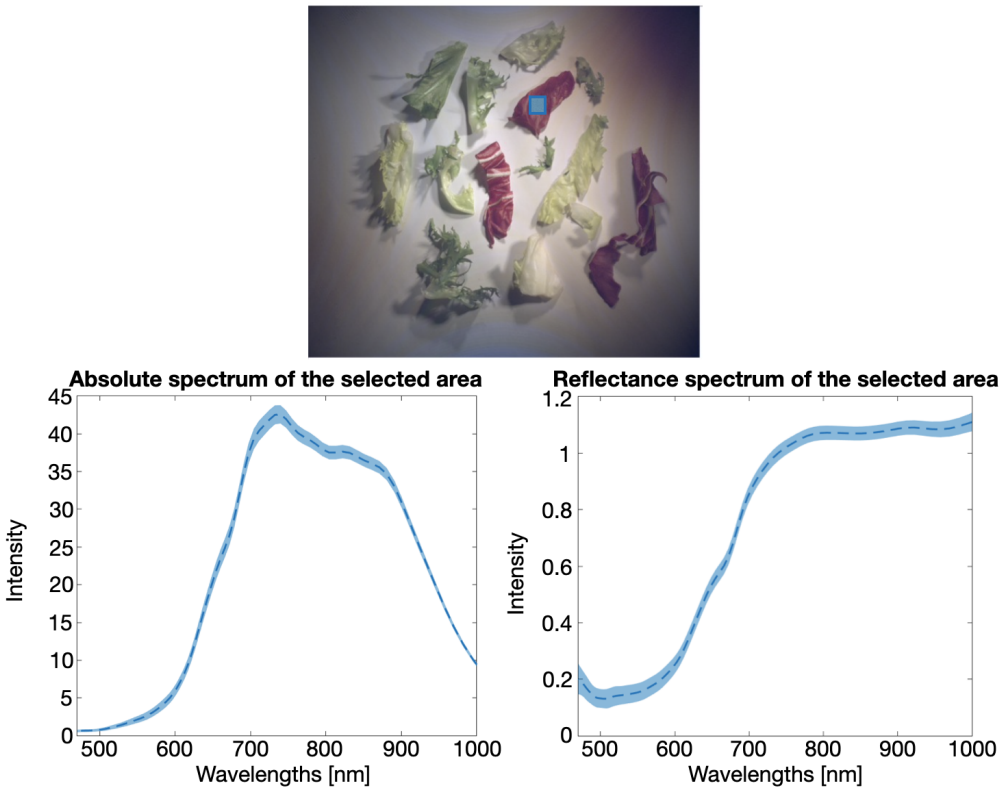

Figure 3.1: Absolute and reflectance spectrum for the area highlighted in blue. The spectrum has been calculated mediating over the spectra of all the pixels in the area. The shaded area represents the standard deviation.

Clearly a low intensity in the reflectance spectrum indicates that the corresponding wavelength is absorbed by the sample, on the contrary a high reflectance intensity shows that the wavelength is reflected.
All the previous considerations are valid also when we are referring to a fluorescence spectra, which should be normalized as well to take orientation and illumination into account and compare spectra of different samples.

3.2 Principal Component Analysis (PCA)

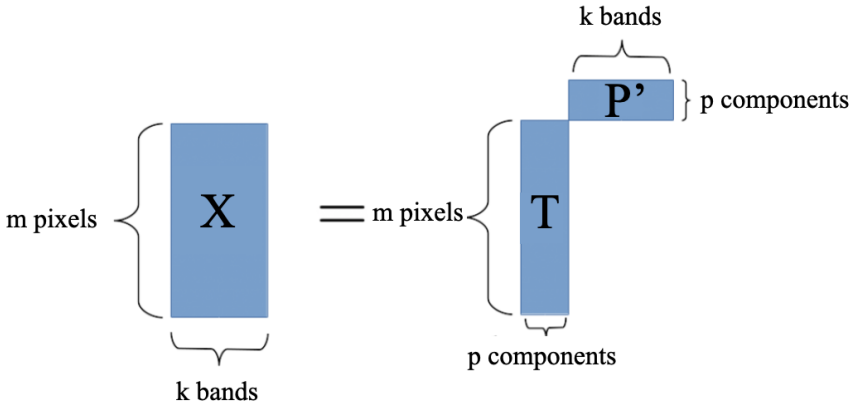

Figure 3.2: Scheme of the PCA matrix factorization.

When such a great number of information is provided like in hyperspectral imaging, it is crucial to understand which one are relevant and distinguish them from the negligible ones. The main goal of Principal Component Analysis is dimensionality reduction, a feature that can be particularly useful in the context of hyperspectral imaging. The hyperspectral cube is a matrix of dimensions $[N_x \times N_y \times N_\lambda]$ which can be rearranged as a matrix $X = [m \times k]$ where $m = [N_x \times N_y]$ represents the number of pixels. The rows of the 2D matrix X therefore, represent the spectrum of the corresponding pixel. Once obtained the reshaped matrix, the central idea of PCA is to obtain dimensionality reduction for the interrelated variables, retaining as much as possible the variation which is present in the dataset. This is obtained by expressing our data with a new set of uncorrelated variables, ordered in such a way that the first few retain most of the variation present in the original ones [17]. Following this approach the matrix X can be factorized as [6]:

$$X = TP^T \tag{3.2}$$

where T is a $[m \times p]$ matrix with mutually orthogonal columns. In T, for each pixel m is reported the intensity for each p component. Instead, the P matrix has dimensions $[k \times p]$ and orthonormal columns. P therefore represents the weights of the original components with respect to the new principal ones. The graphical representation of the previous matrix factorization in provided in Figure 3.2. In this method, the spectrum of any pixel can therefore be expressed as a linear combination of the spectral basis vectors in P. When we consider $p = k$, the PCA is an exact representation of the original matrix X. On the other hand, if the matrix is truncated to $p < k$, assuming to keep only the first components retaining the maximum variance, a dimensionality reduction is obtained. Moreover, we can consider to perform this reduction of variables without loss of information, since the remaining $k - p$ components can be discarded as noise. Later in the work, it will be clear why PCA is a useful tool in hyperspectral imaging analysis. For example, it might indicate important features which enable classification in different components of the same image or distinction of classes in different images. What is important to note however, is that the physical meaning of what the principal components represent is not trivial. The PCs are in general a mathematical tool to maximize variance between data. Interestingly, a p-component PCA of a matrix is the best possible rank p approximation of the data set [6].
To better understand how PCA can be performed on a hyperspectral image and how information can be extracted from this calculations, the algorithm has been performed on the lettuces' image, already analyzed in the previous section. As explained earlier,

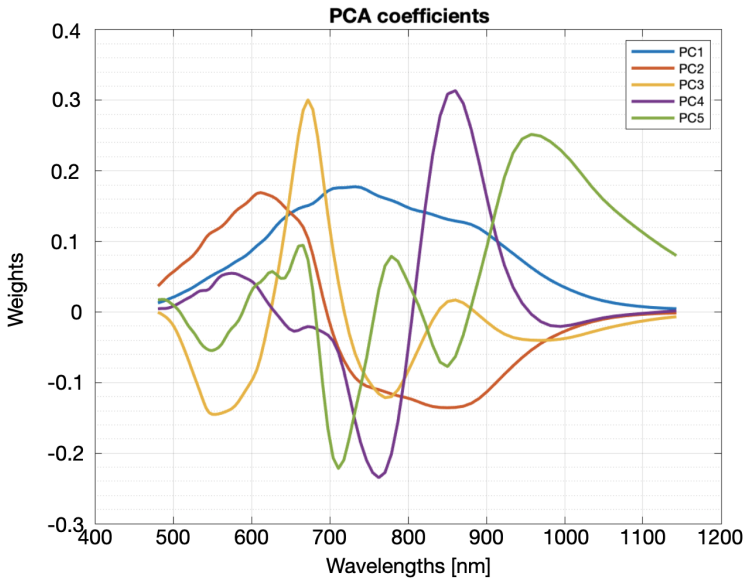

Figure 3.3: Weights for the first 5 Principal Components.

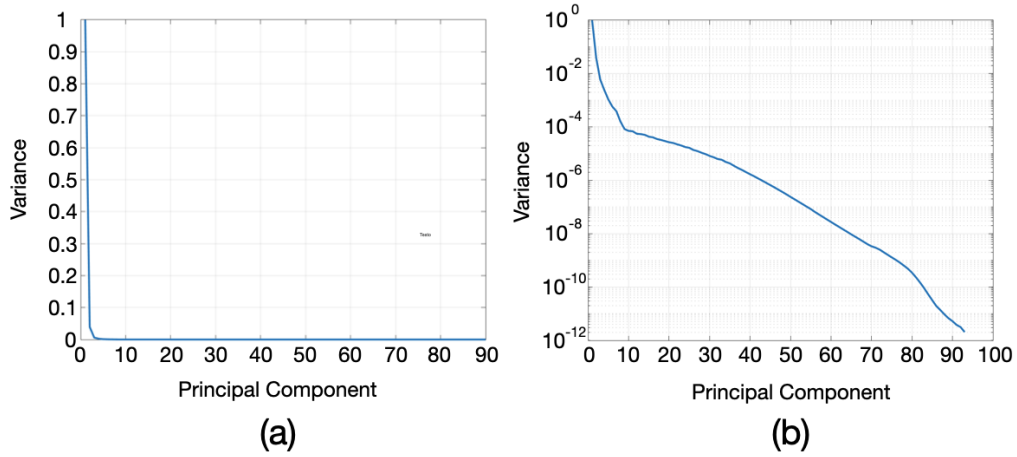

Figure 3.4: (a) Variance of the PCs in a linear scale. (b) Variance of the PCs in a logaritmic scale.

the algorithm constitutes the principal components as linear combinations of the original bands with proper weights, in order to maximize the variance. This concept is made clear by looking at Figures 3.3 and 3.4. In Figure 3.3, the weights of the considered wavelengths in building up the first 5 principal components is represented. As pointed out previously, the meaning of each component is not clearly understandable and has no physical correspondence. Moreover, from Figure 3.4, it is noticeable that the first 3 PCs retain about the 99% of the variance of the sample, this means that they retain all the relevant information for our analysis, reducing the number of channels to be considered from 120 to only 3. As a final proof of the effectiveness of the algorithm in dimensionality reduction, the original image has been reconstructed both in the red, green and blue channel and in the first 3 PCs. The following images (see Figure 3.5) are greyscale representation of the original one: meaning thay they are a 2D section of the cube along a particular spectral component. The darkest parts of the image do not contain the relative component, on the other hand, the lightest areas have a very high value of that component in their spectrum. Clearly the RGB channels are not enough to exhaustively describe the image, many details are not understandable. Differently, the PC components provide a higher amount of detail and enable to distinguish more features and differences in the image.

From this paragraph, the strength and possibilities of the Principal Component Analysis are clear. It enables both the reduction the dimensionality of the problem, simplifying it, and the detection of the main features of the data set. However, it has a difficult physical interpretation.

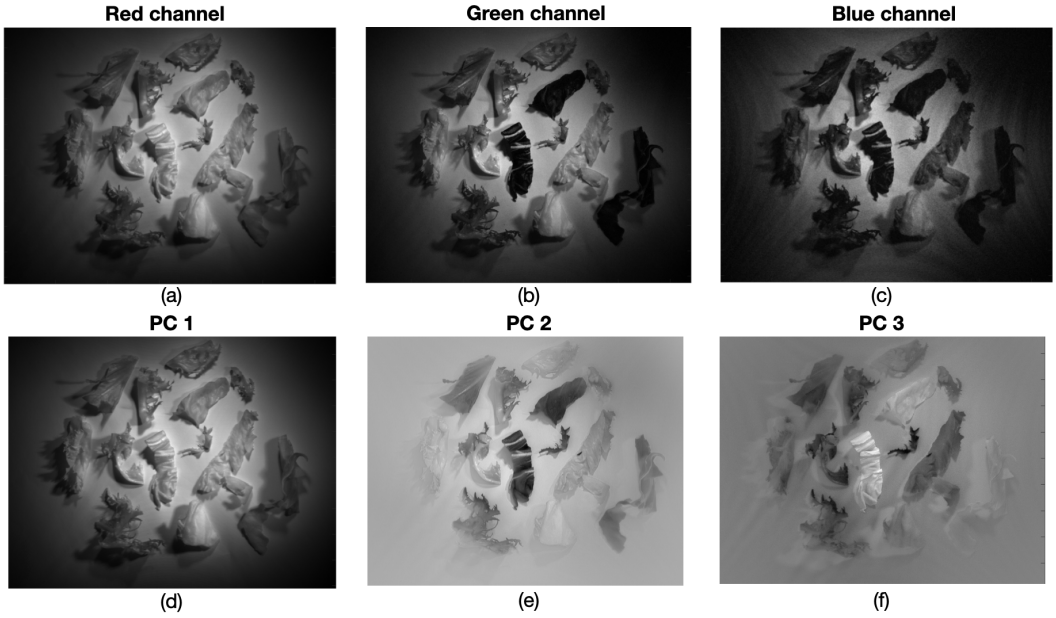

Figure 3.5: (a)-(b)-(c) Red, Green, Blue channel of the image. (d)-(e)-(f) First 3 PCs of the lettuce's image.

3.3 Spectral Angle Mapper (SAM)

The Spectral Angle Mapper is a supervised algorithm that allows to perform clustering in a hyperspectral image. Its basic assumption is that each pixel can be assigned to a single class and there is no overlap between different classes [18]. To assign a pixel to a particular cluster the Spectral Angle Mapper algorithm aim at measuring the similarity between the spectra. This is done by representing each spectrum as a vector in a k-dimensional space, where k indicates the number of bands. The algorithm has to be fed a reference spectra in order to calculate the angle in the k-space between each pixel's spectrum and the reference one. The spectral angle θ is computed mathematically by performing the scalar product between the spectra and dividing it by the product of their norm, finally the *arccos* of this quantity is computed [18].

$$\theta = \arccos\left(\frac{\sum_{i=1}^{nb} s_i r_i}{\sqrt{\sum_{i=1}^{nb} s_i^2}\sqrt{\sum_{i=1}^{nb} r_i^2}}\right) \tag{3.3}$$

where s_i are the components of the pixel's spectrum while r_i are the ones of the reference spectrum. To better understand the procedure underneath the calculations of the spectral angle, a graphical representation of the vector's in the k-space, together with the spectral angle θ between them is reported in Figure 3.6.

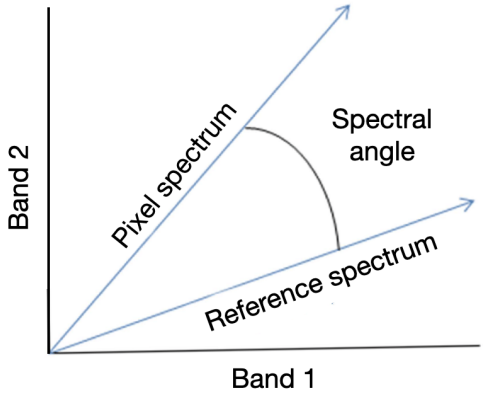

Figure 3.6: Vector representation of two spectra and spectral angle between them.

After calculating the spectral angle relative to the reference spectrum for each pixel, clustering can be performed by setting a threshold for the value of θ and assigning to the same class the pixel whose spectral angle is below the assigned threshold. Indeed, the lower θ, the more the two spectra under consideration will be similar up to the limit where $\theta = 0$: the vectors are parallel in the k-space and the spectra are exactly equal. Being a supervised algorithm, to perform clustering the SAM has to receive as an input the reference spectra, which can be chosen from data provided from literature, previous measurements or directly by selecting a point inside the hyperspectral image to be the

Figure 3.7: (a) RGB reconstruction of the samples and reference pixel. (b) Clustering for a spectral angle threshold $\theta < 0.2$.

reference one. An application of this procedure to the lettuces' samples shown before is presented in Figure 3.7. As a reference, the spectrum of a point inside a leaf belonging to the radicchio species is taken. The algorithm (that is available in the Appendix) performs the calculations of the spectral angles, providing a 2D matrix containing the value of θ for each pixel of the original image. To select the threshold, the data can be plotted in the form of a histogram to better visualize the distribution of the values of the spectral angle in the picture and have a sort of representation of the different clusters (Figure 3.8).

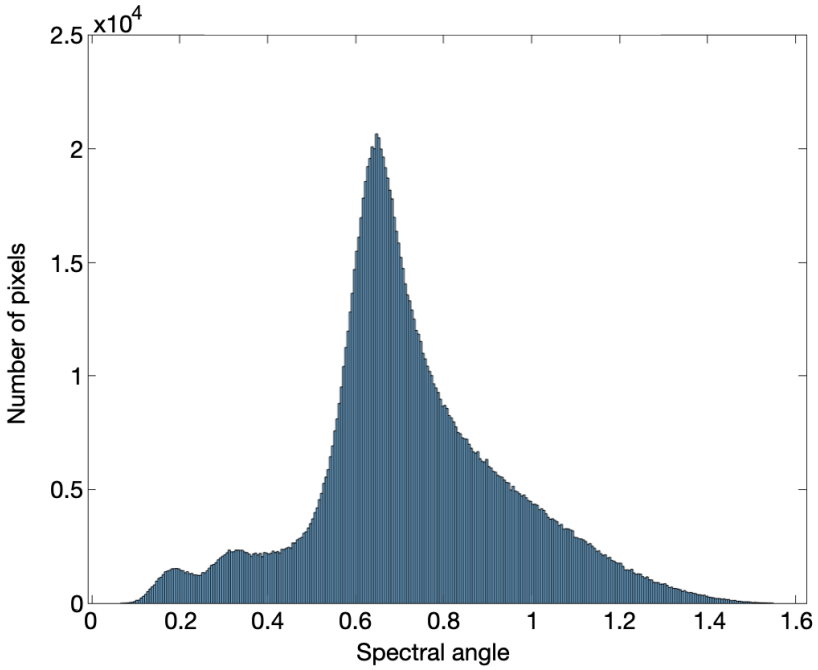

Figure 3.8: Histogram of the spectral angles calculated for the lettuce samples' image.

In the case under consideration, by selecting a threshold $\theta = 0.2$ it is possible to distinguish the leaves of the radicchio species from the other ones as shown in Figure 3.7. By enlarging the value of the spectral angle threshold, more and more pixels will be included in the same cluster of the reference pixel, also the ones referred to other lettuce species. The algorithm can also be exploited, therefore, to distinguish the sample of interest from the background and exclude it from the statistical analysis than can be performed.

The algorithms presented in this chapter have been widely used in the analysis that follow in the work, in particular they have been very useful in detecting the important features to be analyzed and distinguish them from the negligible ones.

Chapter 4

Hyperspectral imaging applications

The global market of hyperspectral imaging system is expected to reach USD 30.0 billion by 2025, at a CAGR (Compound annual growth rate) of 19.3%. This prediction is supported by the growing investments in the field and its employment in a continuously extending number of fields. The numerous applications of HSI technology proof the great flexibility of the technique. In the following sections the most relevant applications of HSI are going to be briefly reviewed with a special focus on food and agriculture: the industry at the center of this work. In particular, we will deal with the analysis of leafy vegetables, which are going to be presented in the last section, together with their most important features that are going to be relevant for the rest of the study.

4.1 Relevant applications

4.1.1 Cultural heritage

Imaging techniques have been employed in the cultural heritage field since the 1990s, however the most conventional ones are not able to provide all the information needed by restorers, curators or archaeologists. Usually these methods are employed as preliminary analysis which are followed by invasive techniques requiring samples or micro-samples from the investigated objects. The development of hyperspectral imaging made possible the realization of very detailed non-invasive analysis and opened the path to various applicative perspective. A first example is the mapping and characterization of pigments of an artwork. In order to employ adequate restoration techniques and avoid damaging the artifact it is crucial to understand the materials and techniques used by the artist or previous restorers. Also, hyperspectral cameras can be employed to moni-

tor the effectiveness of restoration and cleaning processes. When dealing with artworks such as paintings, frescoes or more in general quasi-two dimensional artifacts, imaging is obviously the preferred technique. Well-established traditional methodologies such as ultraviolet-induced fluorescence (UVF), however, provide only partial information, on the contrary HSI techniques can give detailed information on the pictorial materials and their layering. Very interestingly, HSI technologies with suitable sensors, covering the visible (VIS), NIR and SWIR (up to 2500 nm) spectral region, are able to recover hidden layers in the paintings, highlightimg also the underdrawings and *pentimenti* [19]. It is worth to notice that the HERA Iperspettrale has been applied numerous times in the analysis of artworks to investigate the dating of paintings, their attribution and authenticity. A 2020 study conducted by Pelosi et al. [20] for example, employed the HERA camera to investigate the discussed attribution of the "Viterbo Crucifixion" to Michelangelo Buonarroti. The use of the hyperspectral technique enabled the detection in the panel painting of precious pigments, such as ultramarine blue and vermillion, typically employed in the 16^{th} century. This was done by comparing the spectra of colored areas inside the painting with reference spectra available in a public database. Figure 4.1(b) shows a similarity map, obtained with the Spectral Angle Mapper algorithm, applied to the figure of St. John. The red colored areas refer to St. John's mantle, whose spectra shows a strong similarity with vermillion pigment. The green channel considers as a reference spectrum instead one in the fleshy pink tone of the right hand.

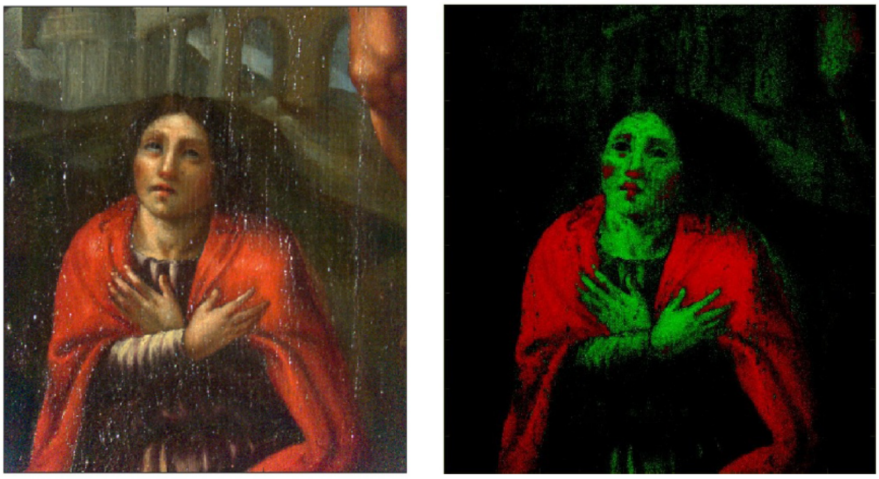

Figure 4.1: (a) RGB reconstruction of St. John's figure. (b) Similarity map for St. John. The red channel is referred to an area in the figure's mantle. Green channel refers to the pink tone in the right hand of St. John.

The figure of St. John is particularly interesting in this painting since its face shows different features under different illuminations. This peculiarity was already demonstrated in other publications [21] and seems an intentional choice of the author since it is only present in this figure. The hyperspectral reconstruction of the image under visible (Figure 4.2(a)) and ultraviolet (UV) illumination (Figure 4.2(a)) highlights the change in the face of St. John,. It appears more feminine with round cheeks under visible illumination and shows a more masculine and thinner aspect when illuminated with UV radiation.

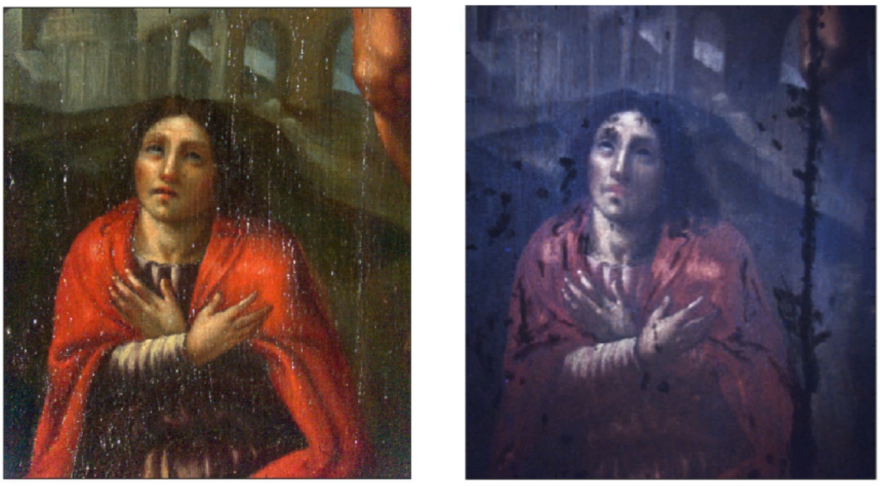

Figure 4.2: (a) RGB reconstruction of St. John's figure under visible illumination. (b)UV illumination reconstruction of St. John's figure.

This example shows how hyperspectral imaging can provide very specific and detailed analysis of artworks in a non-invasive way.

4.1.2 Environmental monitoring

The technological advances in producing small optical elements and building devices with many sensing elements made possible the creation of portable and field-usable HSI technologies. These devices can be exploited in environmental monitoring, either placed on the ground or within UAV (unmanned aerial vehicle) systems. Aerial systems can be employed for example to monitor areas of vegetation, detecting stresses such as drought or pest outbreak. As we will see later, control of plant wellness can be carried out through the examination of particular pigments such as chlorophylls. Applications of UAV hyperspectral systems also include the control of protected environments, for which the characteristic of non-invasivity is crucial, such as glacial regions. Ground-

based HSI devices have instead been used for water quality and pollution monitoring or for detecting micro-plastics contamination in water and soils [22].

4.1.3 Medicine

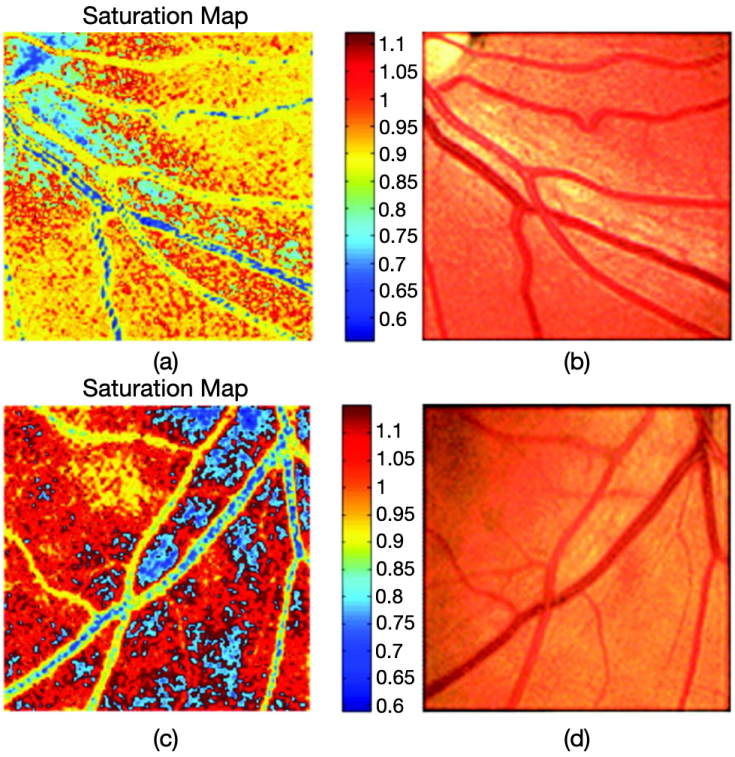

Figure 4.3: (a) Oxygen saturation map and (b) zero-order color image reconstruction of the retina of a 29-year-old healthy male.(c) Oxygen saturation map and (d) zero-order color image reconstruction of the retina of a 58-year-old healthy male.

Medical Hyperspectral Imaging (MHSI) is based on the fact that light propagating in biological tissues undergoes multiple scattering events due to the heterogeneous nature of the biological matrix. The absorption, fluorescence and reflectance characteristic of the tissue can change due to the development of diseases, therefore HSI can be employed as a diagnostic technique which can provide complementary information to the one retrieved from other existing methods. With absorption spectra for example, it is possible to recover the concentration and oxygen saturation of hemoglobin, useful in cancer detection. The potentiality of hyperspectral imaging for disease screening, detection and diagnosis is given by the fact that biomarkers related to particular diseases have specific absorption windows which can be monitored with HSI. As an example Johnson et al.[23]

developed a snapshot HSI system in order to study oxygen saturation inside the human retina. The result of functional mapping of the eye of two healthy subjects is shown in figure 4.3. From these pictures it is possible to appreciate the spatial resolution provided by HSI techniques. Veins, arteries and capillaries are clearly distinguishable from the background. Through this system it is possible to monitor retinal ischemia and arterial or vascular occlusions which are the main cause of untreatable blindness.
Also fluorescence imaging is very useful in this field since cells with different disease states change their rate of metabolisms, giving rise to different fluorescence emission spectra. Finally, providing real-time detailed images, HSI can help the surgeon in image-guided surgery, enabling her/him to better identify ill or damaged tissue [24].

4.2 Food and agriculture

Modern lifestyle puts a lot of attention into the quality and production of the food and goods that are purchased. This requires a constant control from the producer, in order to satisfy the customer's need which are more and more demanding. A primary indicator of a product's wellness is its appearance: size, color, shape, firmness. In order to check on this features many producers still rely on visual inspection performed by an operator. The evaluation in this case is however subjective and limited by human error. The introduction of a reliable, reproducible and fast procedure for quality-checking is crucial to fulfill today's standards. Hyperspectral imaging proposes itself as a perfect tool for the aforementioned needs, guaranteeing an even better source of information, providing a complete and broad spectrum relative to the sample in analysis. An RGB camera would be enough to simply analyze the visual features of the samples, however, the attention of the customers nowadays is not only related to the appearance of the product but also to its nutritional values, nutrients and chemical composition. These features are usually controlled by means of physical or chemical analysis, which are in general time-consuming and destructive, moreover, they refer only to a portion of the sample. Through hyperspectral imaging it would be possible to control, all within the same measurement, both the visual appearance and internal composition of the whole product. That is because particular nutrients have specific absorption windows and the light scattered on the sample provides information on its density and physical structure [25]. Another advantage of the application of this technology in the food industry consists in the fact that the device can be placed in any point of the production chain, enabling the control of every stage of the process and the screening of a great number of specimens. There is a great variety of examples of application of hyperspectral imaging for food monitoring. It has been applied for example for the estimation of the maturity of red and white grapes, which is linked to the concentrations of phenolic compounds in the fruit's skin [26]. The analysis has been carried out by registering the NIR spectrum of the

samples between 900 nm and 1700 nm and applying PCA algorithms to distinguish the spectral features characterizing the grapes with the best maturity stage. Hyperspectral imaging is effective also in detecting the presence of defects before they become visible by the human eye, indeed they might give rise to alterations in the density or texture of the surface of the sample. For fruits and vegetables, defects detection is particularly important, not only from the aesthetic point of view but also from the safety one. A lesion on the skin indeed enhances the probability of pathogen contamination [27]. The fast removal of a damaged sample avoids the contamination of the other ones and prevents the producer from throwing away a bigger amount of products. Examples of this application are studies on the detection of bruises [28]-[29] or chilling injuries on apples [30]. As a proof of the flexibility of this technique, studies with many kind of food can be found in literature, from an analysis for intramuscular fat distribution in beef [31], enabling to determine the quality of the meat, to a non-destructive test able to determine the internal quality of eggs through hyperspectral imaging [32].

4.2.1 Leafy vegetables

In the following sections, the application of hyperspectral imaging to leafy vegetables will be deepened. This kind of food is particularly delicate and highly perishable, the non-invasivity of this technique is therefore especially important. To confirm the importance of this kind of analysis it is interesting to note the growing number of papers that are being published related to hyperspectral imaging applied to species such as spinach [4], lettuce [3]-[2] and leafy vegetables in general [1]. The strength of this technique lays in the fact that it is possible to detect senescence or illness signs in the sample spectra in advance with respect to visual monitoring of the plant. By employing this technology the producer might therefore be able to recover the health status of the vegetable or change the growing conditions to make the plants stronger. Information about the chemical composition and nutrients concentration can be retrieved from the spectrum, such as the chlorophylls, anthocyanin and phenol concentration. These nutrients are fundamental in the growing of the plant and give numerous information on its health condition. Chlorophylls play an essential role in the photosynthesis of the plant, other than being responsible for leaf greenness. These pigments indeed convert the energy coming from solar light in chemical energy to be stored in the plant and the concentration of chlorophylls give an estimation of the photosynthetic potential and nutrient status of the vegetable. Anthocyanin instead, are pigments responsible for the red coloration of plants, however they are also able to reduce the amount of solar radiation reaching the photosynthetic apparatus. For this reason, their production is also linked to stress and illness. From literature it is possible to see that these meaningful nutrients have specific absorption peaks in the VIS-NIR spectral region: chlorophylls absorb at around 670-680

nm while anthocyanin have an absorption peak at around 540-550 nm [33]. We are thus able to link the intensity of these absorptions with the concentration of the corresponding nutrient. For doing so, some indices have been developed throughout various studies and are nowadays a common ground for the determination of important parameters that give information on the wellness of the plant [34],[35]. The most important Vegetation Indices (VI) [36] are listed hereafter where $\rho_{wavelength}$ represents the value of the reflectance spectrum at the specific wavelength:

- **NDVI** (Normalized Difference VI): indicates the general wellness and firmness of the plant.

$$NDVI = \frac{\rho_{800nm} - \rho_{680nm}}{\rho_{800nm} - \rho_{680nm}} \tag{4.1}$$

- **mCARI** (modified Chlorophyll Absorption Ratio Index): is related to the chlorophylls concentration in the plant.

$$mCARI = \frac{1.5 * [2.5 * (\rho_{800nm} - \rho_{670nm}) - 1.3 * (\rho_{800nm} - \rho_{550nm})]}{\sqrt{(2 * \rho_{800nm} + 1)^2 - (6 * \rho_{800nm} - 5 * \rho_{670}) - 0.5}} \tag{4.2}$$

- **mARI** (modified Anthocyanin Reflectance Index): indicates the anthocyanin concentration.

$$mARI = (\rho_{Green}^{-1} - \rho_{Red}^{-1}) * \rho_{NIR} \tag{4.3}$$

- **REP** (Red Edge Position): indicates the position of the wavelength at which the chlorophyll becomes transparent and does not absorb light anymore. Usually it is located at around 700 nm and moves to higher wavelengths for degraded plants.

$$\rho_{re} = \frac{(\rho_{670nm} + \rho_{780nm})}{2} \tag{4.4}$$

$$REP = 700 + 40 * \frac{\rho_{re} - \rho_{700nm}}{\rho_{740nm} - \rho_{700nm}} \tag{4.5}$$

- **CUR**(Curvature Index):

$$CUR = \frac{\rho_{675nm} * \rho_{691nm}}{\rho_{683}^2} \tag{4.6}$$

All of these indices have been formulated by connecting some physical or chemical properties of the plant to some features of the spectrum, more commonly to some intensity values in the reflectance spectrum of the leaf. Even if the relationship of the index with the corresponding meaningful quantity is not always linear, it represents a good indicator of the relative characteristic. In the following analysis the HERA camera will be employed to analyze the health status of different species of leafy vegetables, both before and after harvesting. The spectral range of the HERA Iperspettrale (400 - 1000 nm) in

the VIS-NIR is useful in determining both the visual aspect of the leaves and their nutrients' concentration. Moreover, we're able to perform also hyperspectral fluorescence measurement which are particularly relevant in plant analysis. Chlorophylls are indeed fluorescent molecules and from these measurements we obtain the whole fluorescence spectrum that is able to provide more information than a single value of chlorophylls concentration obtained with more conventional techniques. As will be clear later, the strength of performing a measure providing the full spectrum of the image is that, having such a big amount of information which are related to different leaves at various health condition, new indices similar to the one considered before can be developed, depending on the specific case under consideration.
From literature, the general behavior of a healthy plant spectrum compared to a degraded one is know and is represented in Figure 4.4 taken from the study of Simko et al. [3] on the decay of fresh-cut lettuce. The general trend for the spectrum of a senescent leaf shows a decrease of reflectance in the NIR region (around 700 nm) and, for green leaves, the vanishing of the peak in the green spectral region. We will see later, that actually the evolution of the spectra due to senescence greatly depends on the species taken into consideration and on their conservation technique.

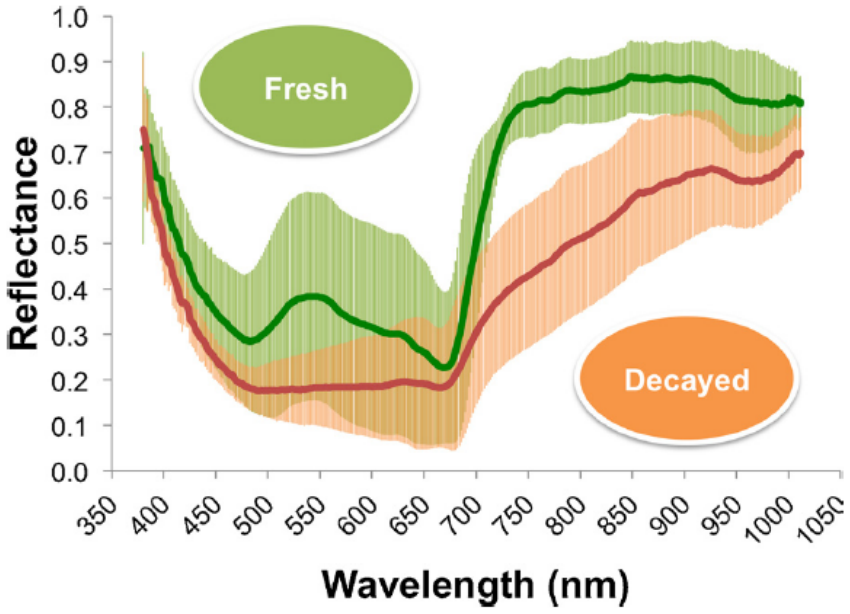

Figure 4.4: In green the spectrum relative to a healthy leaf. In red is represented the spectrum of a degraded one.

Chapter 5

Results of HSI analysis in vertical farming

In this chapter the main results of a collaboration project between NIREOS and Agricola Moderna, a vertical farm based in Milan, are going to be presented. Different species of leafy vegetables produced by Agricola Moderna have been analyzed with the HERA Iperspettrale. The main goal of the study consisted in the detection of spectral features characterizing the growth and senescence of the plants. The measurements were performed with different growing and conservation techniques. Both reflectance and fluorescence measurements have been taken into account to evaluate the health status of the specimens. These indices of well-being or stress of the leaves could be applied in the future to monitor the life-cycle of the plants in Agricola Moderna's facilities.

5.1 Leafy vegetables' shelf life

A crucial parameter for food products is the determination of their *shelf life*: the maximum amount of time between production and consumption which guarantees its safety without risks for the consumer. In this experiment, the senescence of three different species of leafy vegetables has been monitored in different conservation techniques to detect early signs of degradation in their spectra. The result of the data analysis is presented in this section. Leaves belonging to the species under analysis are shown in Figure 5.1: the green leaf on the upper left is a *Celinet* lettuce, while the one on the right is a *Wasabina* leaf, the red leaf instead belongs to the *Komatsuna* species.

Figure 5.1: Leaves of Celinet lettuce, Wasabina (on top) and Komatsuna variety (below).

In the following sections, hyperspectral data for three different conservation techniques of the aforementioned leaves will be presented. The harvesting of all the samples in this study took place the day before the beginning of the measurements: we were thus able to follow the whole senescence process of the plants. The experimental setup presented in the next section is common to all the measurements.

5.1.1 Experimental setup

Figure 5.2(a) shows the experimental setup for reflectance measurements. The HERA camera is placed on a tripod and set above the sample, at about 130 cm distance. The scene is illuminated with two 20-W halogen lamps, placed above the specimens to guarantee the most homogeneous illumination possible. The lamps are placed at a distance of around 1 m from the leaves in order to avoid heating and subsequent damaging of the sample. The HERA camera is connected to a computer via USB and measurements parameters can be set with an acquisition software. These parameters include the integration time, the number of averages (meaning the number of images taken for every step of the interferometer, which are then mediated to obtain the final data) and the spectral resolution. Finally, on top of the HERA are placed two sliders which enable the manual tuning of the focus and the iris aperture of the camera.

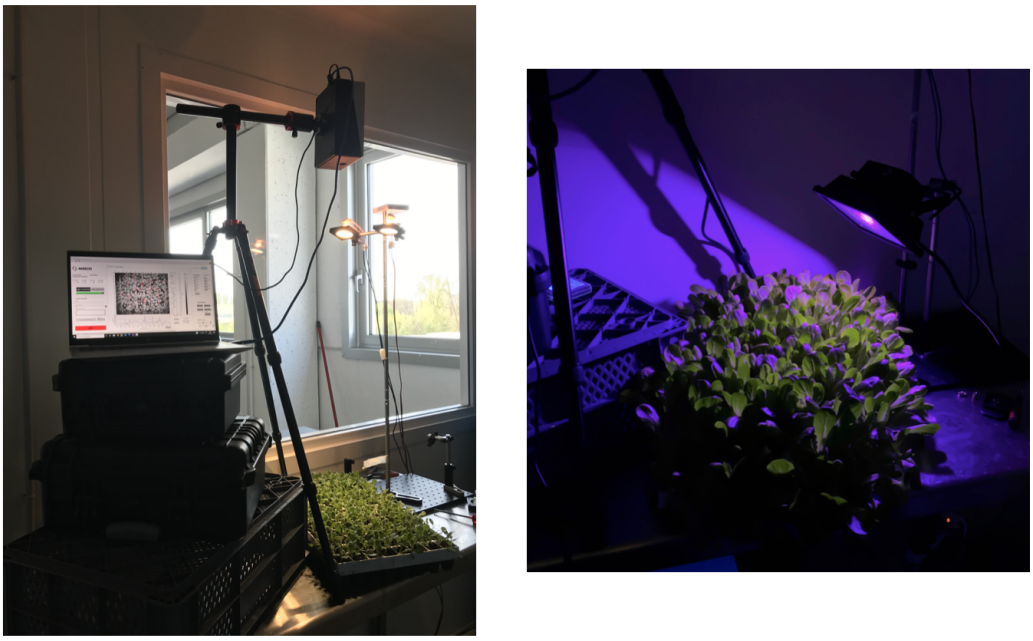

(a) (b)

Figure 5.2: Experimental setup for (a) reflectance measurements (b) fluorescence measurements.

To obtain reflectance data, two measurements have to be carried out for each sample: one on the specimen, to retriece the absolute data cube, and one of a lambertian surface for the normalization. In practice the measurement of a lambertian is done on a white paper which can be assimilated to an ideal diffusing surface. It is important to note that to obtain a good normalization the sheet should be placed on the same focal plane of the specimen.

Experimental setup for fluorescence measurements is shown in Figure 5.2(b). The position of the camera remains unchanged while illumination changes. Samples are excited via a 20-W blue LED at 400 nm placed at about 20 cm from them. A long pass filter is placed in front of the camera in order to cut off excitation light. The fluorescence signal is very weak compared to the reflectance one, therefore measurements in this second case have to be performed in complete darkness apart from the LED source. Integration times are longer to enable the camera overture to capture a higher amount of photons.

In the following sections, the evolution of the spectra due to senescence for the three species in Figure 5.1 will be analyzed. The recognition of trends and spectral features

relatable to physical changes in the sample will be the focus of the analysis. As we will see, the type of senescence process will vary depending on the post-harvest conservation technique of the samples. During the day which occurred between the harvesting and the beginning of the measurements all the samples were conserved at low temperature in a refrigerator. Three different preservation conditions have then been analyzed, varying in particular the temperature of the conservation and the surroundings of the sampled leaves:

- **Conservation method 1: room temperature, separated leaves**. The measured leaves were placed separately on a white paper and kept at room temperature in the laboratory.
- **Conservation method 2: low temperature, grouped leaves**. The leaves were kept together in a plastic box and stored in a refrigerator at $+4°C$.
- **Conservation method 3: low temperature, separated leaves**. Samples were positioned separately on a white paper and stored in the refrigerator at $+4°C$

5.1.2 Conservation method 1

Samples for these measurements were selected among the harvest from visual inspection, picking leaves that seemed healthy and with a lively hue. A single leaf was selected for each species under investigation and stored at room temperature. Hyperspectral images of the samples were taken always in the same measuring conditions, until the vegetables were visibly degraded and no more edible. Obviously this preservation method is not adequate for perishable samples like leafy vegetables, therefore we expect them to have a very fast degradation process and to show quite early signs of illness or senescence. Moreover, since they're kept isolated one from each other, we don't expect a single leaf's degradation to be influenced by the presence of the others. In Figure 5.3, the reflectance spectra referred to the three species at 0, 4, 24 hours after harvesting are displayed.

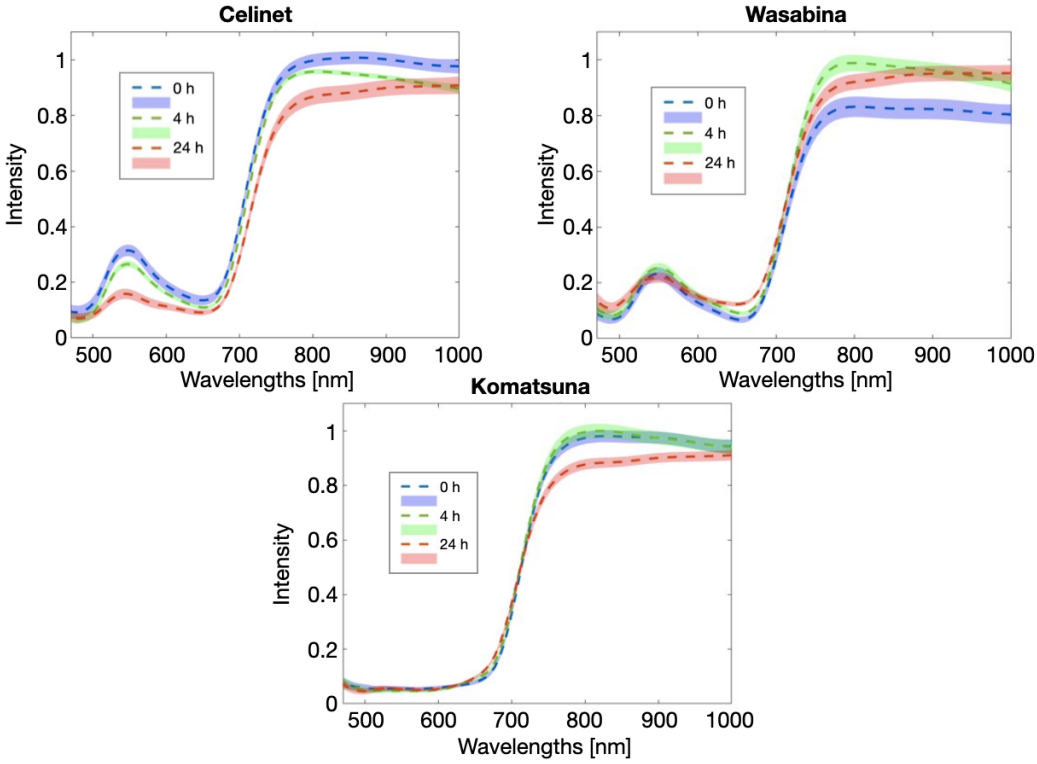

Figure 5.3: Reflectance spectra for the three species 0, 4 and 24 hours after harvesting are represented respectively in blue, green and red. Shaded areas represent the standard deviation of the spectrum.

Each spectrum has been calculated by performing the mean over the pixels of a manually selected area inside the corresponding leaf. The portion of the leaf was chosen in order to adequately represent the overall health condition of the sample. The first analysis

performed on the obtained data consisted in the visual inspection of the spectra to detect either common behaviours or evident differences.In the visible range it is possible to note that the green peak of the Celinet almost vanishes in 24 hours, clearly representing a senescence sign for this species. On the other hand the spectral behaviour of the other species in the visible range seems unchanged. These trends suggest that the Celinet leaf should present an altered hue due to degradation while the color of the others should remain almost unchanged.

Figure 5.4: RGB reconstruction of the samples at 0, 4 and 24 hours in the senescence process.

These predictions are actually confirmed by visual inspection of the samples, as can be seen in Figure 5.4. The Celinet leaf on the top left becomes darker and darker with time, meaning that the green wavelengths are more strongly absorbed. The Wasabina and Komatsuna variety, on the other hand, retain almost the same color throughout the senescence process. Going back to the spectral signature, a common trend for all the species seems to be their behaviour in the NIR region. To better understand the

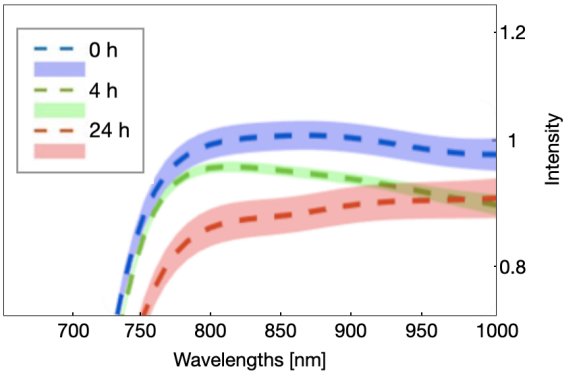

Figure 5.5: Representation of the NIR region for the Celinet species.

following observations, an enlargement of the NIR spectral signature for the Celinet leaf is shown in Figure 5.5. When looking at reflectance spectra, it is important to remember that more than their relative intensity, it is their shape that matters. The intensity is indeed related to the strength of the illumination. In the present case for example, it is possible to notice that all the blue spectra remain flat in the NIR after 825 nm (see Figure 5.5). Looking at the behaviour 4 hours after harvesting instead, we can note an absorption signature in the infrared region with respect to the plateau in the 825 - 875 nm range. On the contrary, the red spectra all register an enhancement in the reflectance intensity after the flat region around 825 nm.
As introduced in Chapter 4, the rule of thumb to connect spectral behaviours with observables is to create a reproducible index. In order to quantify and try to confirm the predictions obtained with visual inspection, an index has been developed to describe the strength of the absorption in the region around 970 nm with respect to the plateau around 825 - 875 nm:

$$NIR_{index} = \frac{\rho_{825-875nm}}{\rho_{960-1000nm}} \tag{5.1}$$

Interestingly, it is known from literature that water has an absorption window around 970 nm. Figure 5.6 shows indeed the absorption coefficient of water (from Palmer and Williams, 1974 [37]), where a peak at 970 nm is clearly distinguishable. The other absorption peaks of water reside at longer wavelengths, we will see in Chapter 6 the possibilities of analysis in the Infrared spectral region.

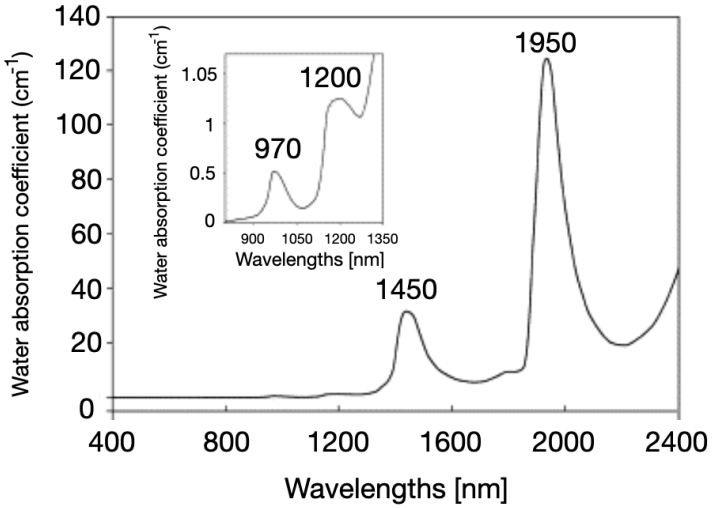

Figure 5.6: Water absorption coefficient from Palmer and Williams, 1974.

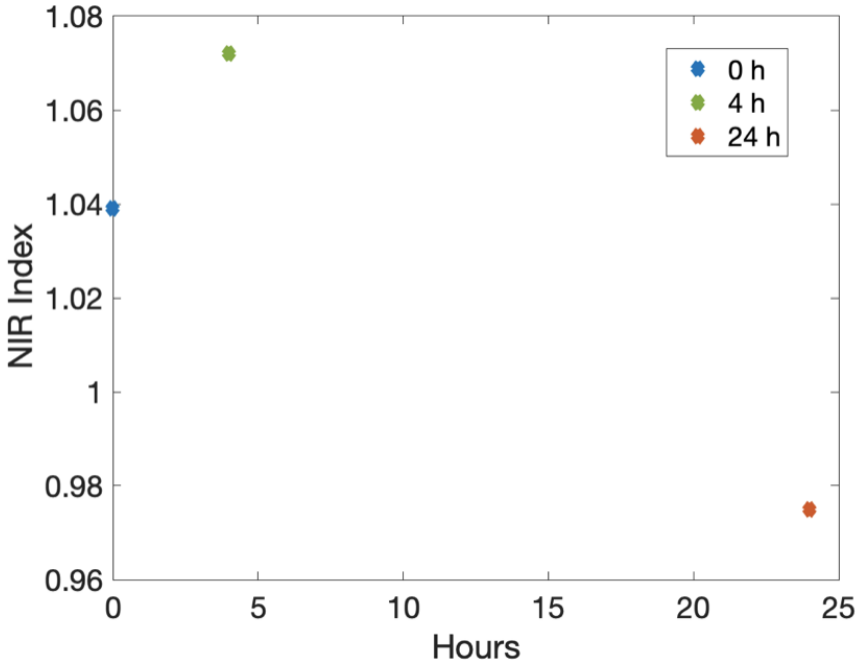

Figure 5.7: NIR index calculations for the Celinet leaf obtained from the previously collected hyperspectral measures.

We can therefore link the newly introduced NIR index with the presence or absence of water in the plant, indicating its hydration condition. As shown in Figure 5.4, throughout their degradation process the leaves lost their firmness and after 4 hour they appeared wet. On the contrary, after 24 hours the samples were completely dehydrated and brittle. This process is correctly represented by means of the NIR index which is reported in Figure 5.7 in the case of the Celinet leaf. A similar trend was then observed for the other species. A NIR index greater than 1 indicates absorption in the 960 - 1000 nm spectral range, most likely linked to the presence of water. The increase of this quantity between data collected at 0 and 4 hours after harvesting correctly suggests that in this time interval the leaf releases the water contained in it. The sudden drop between the index calculated 4 and 24 hours into the measurement campaign correctly reproduces the observed dehydration of the leaves due to senescence.

The analysis of these first samples show that the spectra correctly represent the physical process of senescence of the species. The kind of degradation varies depending on the species, even if some common behaviour can be recognized. The development of the NIR index finally enables the prediction of the hydration status of the plants. With respect

to the shelf life, as expected the samples under consideration experienced a very fast senescence process, indicating that clearly this conservation technique is not suitable for a good preservation of leafy vegetables.

5.1.3 Conservation method 2

In the second round of measurements the samples were stored together in a sealed plastic box placed in a refrigerator at $+4°C$ which was extracted only for the measurements. In this case we expect to obtain a longer shelf life since this conservation technique seems adequate for the correct preservation of the leaves. We suppose also that there is some kind of interaction in the senescence process of the leaves, since they are stored together. Hyperspectral images were taken in the same measuring conditions as the ones of the previous study at intervals of about 48 hours, monitoring the evolution of the whole senescence process. Figure 5.8 shows the spectra referred to the 1^{st}, 12^{th} and 19^{th} day after harvesting.

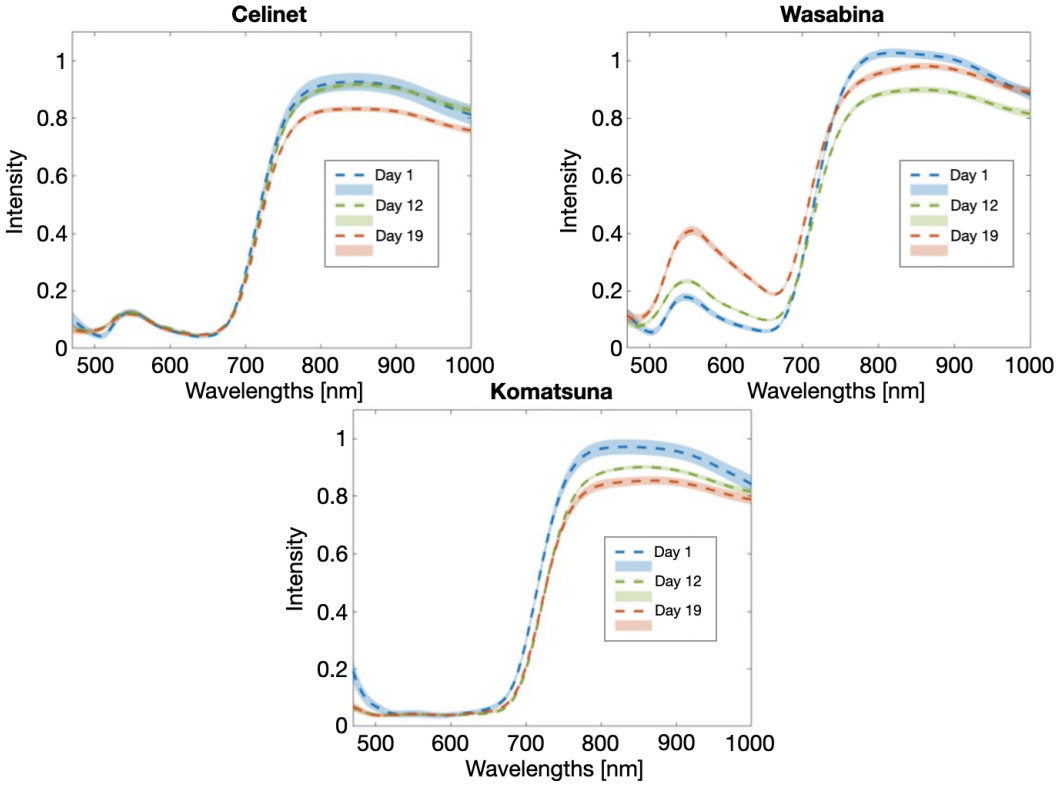

Figure 5.8: Reflectance spectra for the three species collected on the 1^{st}, 12^{th} and 19^{th} day after harvesting are represented respectively in blue, green and red. Shaded areas represent the standard deviation of the spectrum.

Similarly to the previous measurement campaign, the spectra represented in the figure have been obtained by choosing a reference leaf in the box for each species and calculating the medium spectrum for a selected area in the sample. In this case only the

Wasabina spectra show a variation in the visible range, characterized by an increase in the reflectance in the green spectral region and a shift towards higher wavelengths of the peak. The other species instead do not show significant changes in the VIS. Visual inspection of the sample confirms the predictions of the hyperspectral analysis. The Wasabina leaf indeed shows a gradual shift of its hue from greenish to yellowish. Interestingly this shift is way more visible in the spectra than from the pictures as shown in Figure 5.9.

Figure 5.9: RGB reconstruction of the Wasabina leaf on the 1^{st}, 12^{th} and 19^{th} day in the senescence process.

Focusing the attention on the NIR region, It is worth noticing that also in this case all the specimens show a similar spectral trend, highlighted in Figure 5.10.

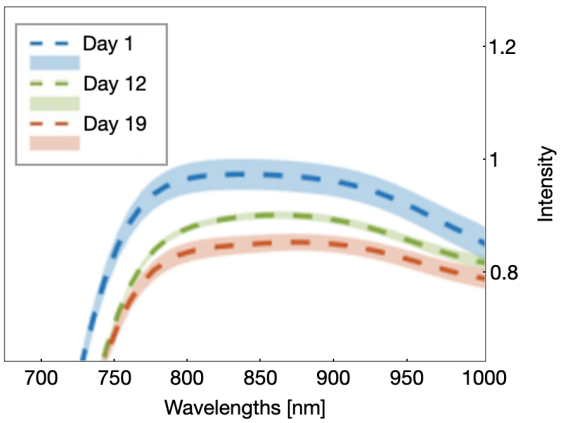

Figure 5.10: Representation of the NIR region for the Komatsuna variety.

The strong absorption in the region around 970 nm that characterizes the spectra related to the 1^{st} day post-harvest diminishes with time with respect to the plateau at 825 - 875 nm. Figure 5.11 plots the NIR index developed in the previous section related to

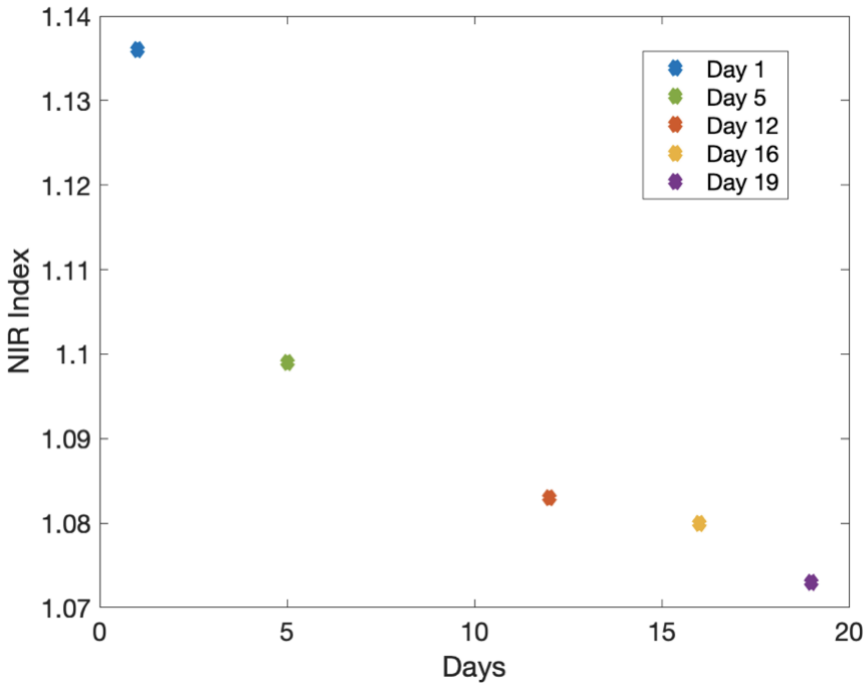

Figure 5.11: NIR index calculations for the Wasabina leaf obtained from the previously collected hyperspectral measures.

the spectra of the Wasabina leaf for five different measurements. The trend of the NIR index confirms that the water-related absorption at around 970 nm diminishes as the senescence process of the leaves goes on. This trend is observed also in the other species, indicating that all of them undergo a process of dehydration. This result is again confirmed by visual inspection of the samples which on the last day of measurement present themselves as very dry. However, they do not ever become as brittle as the samples considered in the first measurement campaign, as can be understood by the fact that the NIR index never reaches a value smaller than 1.

Also fluorescence measurements, with the experimental setup earlier described, have been performed on this samples. These experiments showed very interesting results that will now be presented. Figure 5.12 shows the fluorescence spectra for the Wasabina, Celinet and Komatsuna variety on the 1^{st}, 12^{th} and 19^{th} day of the measurement campaign. As already pointed out in Chapter 4, important nutrients inside plants are also fluorescent molecules. The principal peak around 750 nm indeed, highly visible in all the species, is relatable to the concentration of chlorophylls in the leaves. All the spectra experience a decrease in the chlorophylls' peak intensity as degradation goes on, indicating

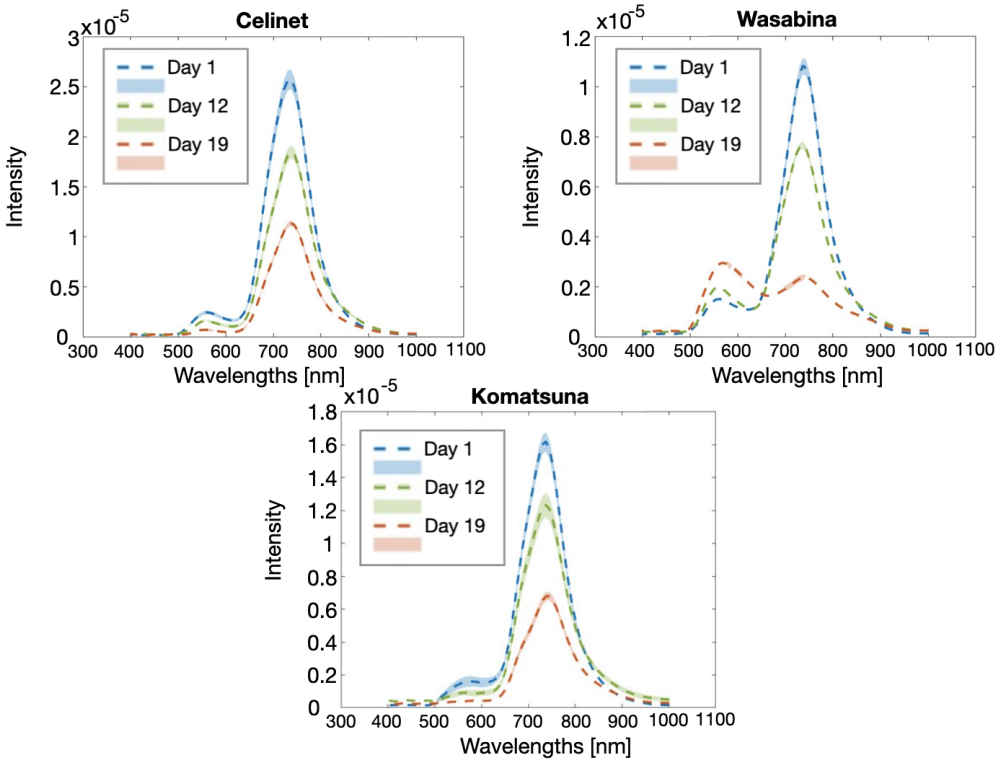

Figure 5.12: Fluorescence spectra for the three species collected on the 1^{st}, 12^{th} and 19^{th} day after harvesting are represented respectively in blue, green and red. Shaded areas represent the standard deviation of the spectrum.

a lower photosynthetic potential and a clear sign of senescence. A secondary peak is also noticeable in the spectra in the figure at around 550 nm. Interestingly, the three species show different behaviour with respect to the evolution over time of the intensity of this secondary peak: it increases in the Wasabina species while it has a decreasing trend for the Celinet and Komatsuna leaves. Literature research shows that a fluorescence peak around 550 nm is characteristic of phenolic compounds [38]. Phenols are responsible for the antioxidant properties of many leafy vegetables, however their production is also linked to plant stress and senescence. Spectra in Figure 5.12 therefore suggest that the Wasabina species increases its phenols production during degradation, on the other hand the phenolic compounds inside the Celinet and Komatsuna do not seem to have a major role in the senescence process. Differently, the decrease of chlorophylls concentration seems to be an important sign of degradation of the plant, moreover it is common to both the species analyzed. To quantify the presence of chlorophylls inside the leaves, a Chlorophyll Index, similar to the one introduced in Chapter 4 , has been employed. The Chl_{index} links the intensity of the reflectance spectrum at around 670 nm (corresponging

to a chlorophyll absorption peak) to the concentration of the nutrient:

$$Chl_{index} = 1 - \frac{\rho_{660-680nm}}{\rho_{760-800nm}} \tag{5.2}$$

The equation above has been applied to a portion of the hyperspectral image corresponding to the same Wasabina leaf displayed in 5.9. Figure 5.13 reports a reconstruction of the leaf based on the value of the chlorophyll index on the 1^{st}, 12^{th} and 19^{th} day post-harvest. The color-bar on the right relates the color of the image with the value of the chlorophyll index.

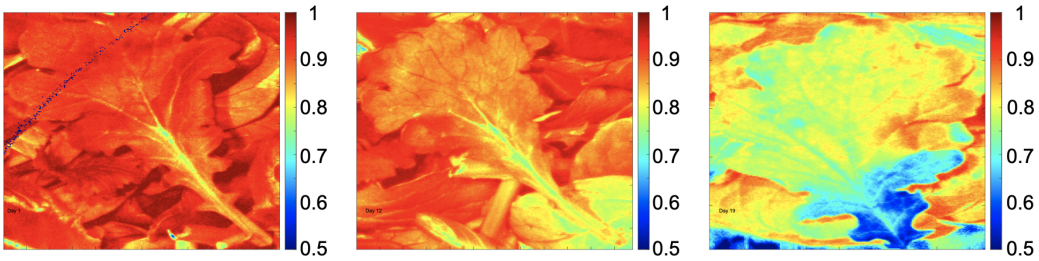

Figure 5.13: Reconstruction of the wasabina leaf based on the Chl_{index} intensity. The colorbar shows the value of the index corresponding to colors in the figure.

Clearly the value of the chlorophyll index, related to the nutrient's concentration in the leaf, diminishes as the senescence process goes on. From Figure 5.13 we can also appreciate the incredible spatial resolution of the HERA Iperspettrale. Indeed through this visual reconstruction starting from the hyperspectral data we're able to finely distinguish the details of the different parts of the leaves, from the stem to the venation.

The second conservation method, analyzed in the current section, resulted very effective in extending the shelf life of the samples which were preserved for around 20 days. The different storage resulted in a different degradation process with respect to the one of the previous technique. In particular, the common trend that characterized senescence in this case was the dehydration process, correctly depicted by the NIR index. Fluorescence analysis resulted particularly effective in detecting another important degradation index: the decrease of chlorophylls concentration.

5.1.4 Conservation method 3

For the last set of measurements, separated leaves were kept in the refrigerator at $+4°C$ inside sealed plastic boxes and extracted only for the hyperspectral measures. The conservation condition is therefore very similar to the previous one, apart from the fact that the leaves are not stored together, therefore there is no interaction among them. Also in this case we expect a long shelf life. The measurement campaign proceeded simultaneously to the previous one and the measurements were executed during the same days. Spectra for the three species referred to the 1^{st}, 12^{th} and 19^{th} day after harvesting are depicted in Figure 5.14. In this case more than one leaf was selected for each species. The analyzed leaves are represented in Figure 5.15: the two Celinet leaves are shown on the left, two leaves of the wasabina species are located in the middle while three samples of Tatsoi leaves are represented on the right. The spectra in the following figure are the result of the average over manually selected points inside the reference leaves of each species.

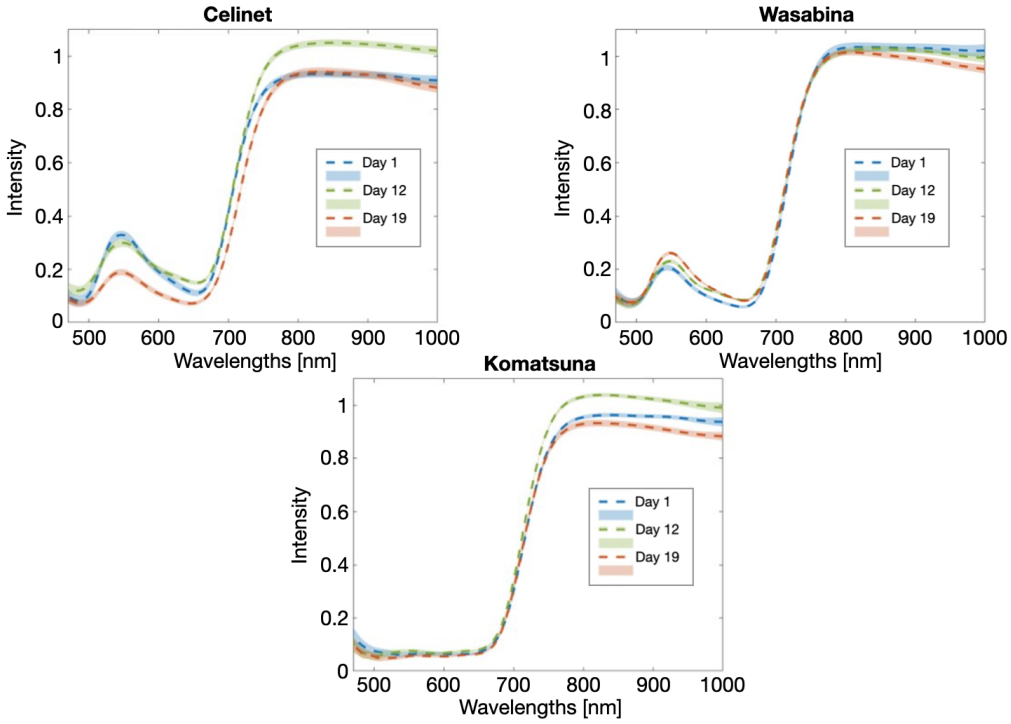

Figure 5.14: Reflectance spectra for the three species collected on the 1^{st}, 12^{th} and 19^{th} day after harvesting are represented respectively in blue, green and red. Shaded areas represent the standard deviation of the spectrum.

From visual inspection of the spectra, it is possible to note that the behaviour in the

visible range of the three species is similar to the one obtained in the first conservation condition. The peak in the green spectral region of of the Celinet species' spectra diminishes over time while there are no relevant changes in the VIS for the other two species. Again the observation of the hyperspectral data correctly predicts the change in the color of the Celinet leaf which gets of a darker shade of green as shown in Figure 5.15. The Wasabina and Komatsuna leaves, on the other hand, do not show a significat change in the hue over the measurement period.

Figure 5.15: RGB reconstruction of the samples on the 1^{st}, 12^{th} and 19^{th} day in the senescence process.

By looking at the NIR behaviour of the three spectra, we can recognize a common trend for all the species. The absorption in the spectral region around 970 nm with respect to the flat region at the beginning of the NIR seems to increase as the degradation of the leaves goes on. A highlight of this observation is depicted in Figure 5.16.

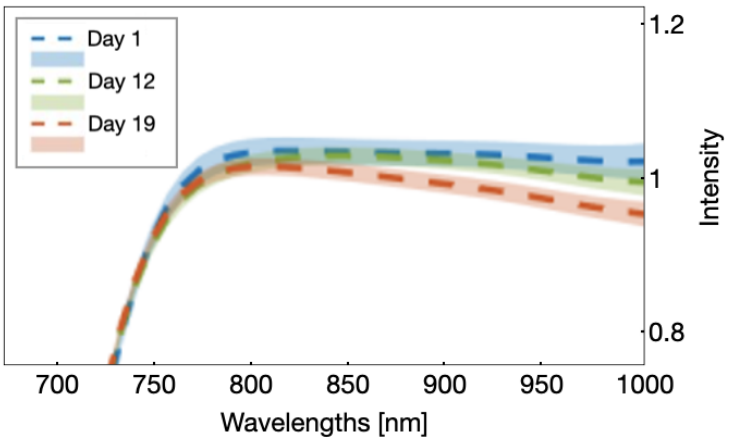

Figure 5.16: Representation of the NIR region for the Wasabina species.

To confirm this hypothesis, which would lead to an opposite behaviour with respect to

the one observed in the previous set of measurements, the NIR index is plotted for five measurements related to the Wasabina species in Figure 5.17.

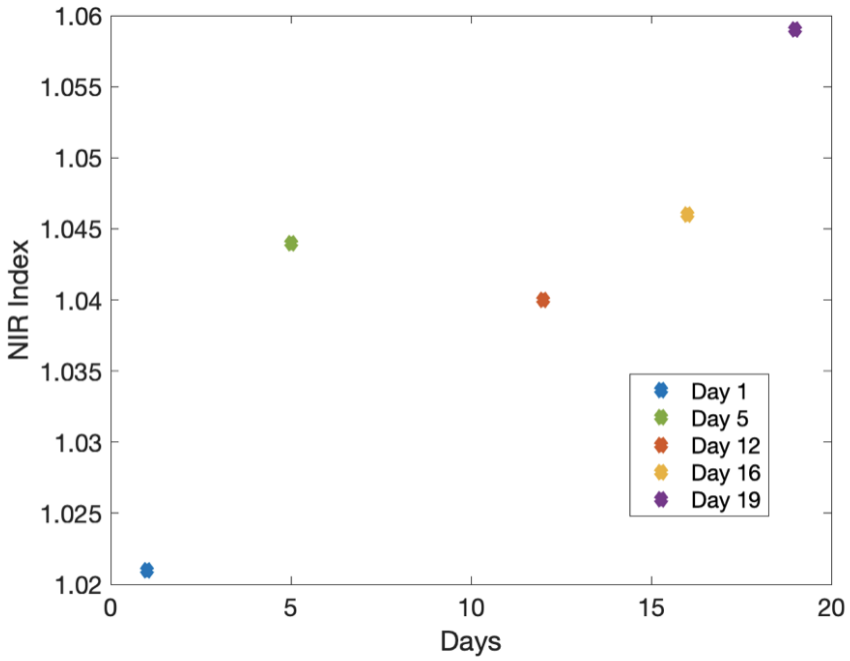

Figure 5.17: NIR index calculations for the Wasabina leaf obtained from the previously collected hyperspectral measures.

The general trend is confirmed by the behaviour of the NIR index which grows over time, indicating an increase in the water-related absorption window. This spectral trend can be connected to the physical observation of the leaves represented in Figure 5.15 which resulted more and more moist throughout the measurement campaign.
Finally fluorescence measurements were performed on the same samples and the retrieved spectra are represented in Figure 5.18. Similarly to the case considered in the previous section, in all the species it is possible to observe a diminished intensity of the fluorescence peak related to chlorophylls concentration at around 750 nm. This spectral behaviour indicates again that the reduced photosynthetic potential is a sign of senescence for plants. To confirm this hypothesis, the chlorophyll index introduced in the previous section was retrieved from hyperspectral data. A reconstruction of the Wasabina leaf on the 1^{st}, 12^{th} and 19^{th} day after harvesting is represented in Figure 5.19. The index retrieved from reflectance data confirms once again the prediction of the fluorescence spectra for chlorophylls concentration. A clear decrease in the nutrient's value is noticeable.

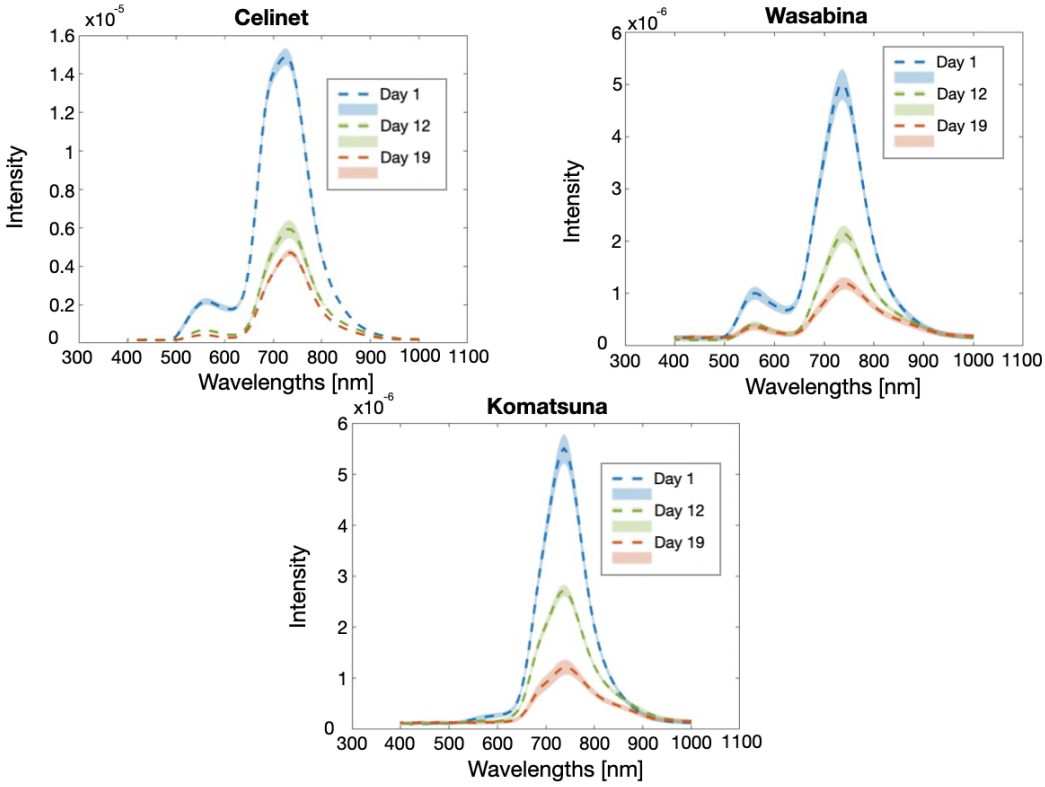

Figure 5.18: Fluorescence spectra for three species collected on the 1^{st}, 12^{th} and 19^{th} day after harvesting are represented respectively in blue, green and red. Shaded areas represent the standard deviation of the spectrum.

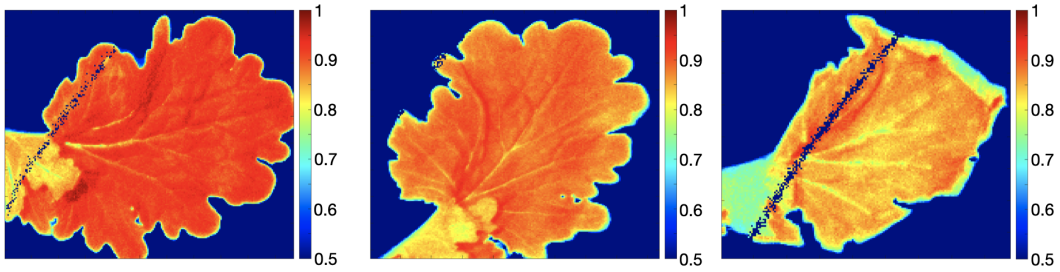

Figure 5.19: Reconstruction of the wasabina leaf based on the Chl_{index} intensity. The colorbar shows the value of the index corresponding to colors in the figure.

In this case the secondary peak linked to the phenolic compounds' concentration diminishes over time for all the species and is almost absent in Komatsuna's fluorescence spectral fingerprint (see Figure 5.18). This behaviour suggests that the increase in the phenolic peak shown in figure 5.12 for the Wasabina species is linked to the yellowing of

its hue, which was only observed in the previous conservation method.

The conservation technique analyzed in this section led to a shelf life of the plants very similar to the one shown for the previous samples of around 20 days. This observation suggests that crucial parameters for a good preservation of leafy vegetables are low values of temperature and humidity which characterize the refrigerated environment. However the environment in which they were kept, meaning if they were isolated or stored together, influenced their senescence process. Degradation was indeed characterized by different spectral and physical features in the different conservation methods.

5.2 Biostimulants' effects on the growth and senescence of plants

In this section a further collaboration project between NIREOS and Agricola Moderna is going to be presented. The effect of the application of biostimulants during the growth of three species of leafy vegetables has been analyzed with hyperspectral imaging. Moreover their effect on the shelf life is studied with techniques similar to the ones presented in the previous sections. Final goal of this study was to understand whether the effect of the biostimulants is relevant and detactable through the spectral fingerprint of the samples. The plants have been grown inside Agricola Moderna's R&D facilities inside three different cells, each one characterized by a different concentration of stimulant substances. All the other growing conditions of the plants were the same. They all received the same amount of light, water and nutrients. We therefore expect that any difference in the growing process would be due to the effect of the biostimulants. Three species of leafy vegetables were taken into account in the study: *Romaine lettuce*, *Green lettuce* and *Tatsoi*. First the analysis will concentrate on the growth of these samples and later on their shelf life.

5.2.1 Biostimulated growth of leafy vegetables

Seeds of each species under consideration were grown in three different cells with decreasing biostimulants' concentration:

- **Cell 1**: biostimulants' concentration of 10 ppm (part per million);
- **Cell 2**: biostimulants' concentration of 1 ppm;
- **Cell 3**: **control**, no stimulants were given to the plants in this cell.

The growing of the samples started from the seeds which were initially kept in a condition of darkness for uniform germination. The first measurements were taken when the plants presented their first leaves, which happened after 7 days in the light. The subsequent measurements took place with an interval of around 7 days in correspondence of the 14^{th} and 20^{th} Day Under Light (DUL). The last measurement on DUL 20 was taken right before harvesting of the samples therefore it was possible to monitor with hyperspectral measures the whole growing process of the plants. In Figure 5.20 spectra referred to the Green lettuce species are presented. Measurements taken on the 7^{th},14^{th} and 20^{th} DUL of the samples are represented respectively in blue, green and red. Different cells instead are distinguished with different type of lines: solid lines refer to the first cell with the highest concentration of hormones, dashed-lined spectra are referred to the second cell with a lower concentration of biostimulants while lines composed of both dashes and dots indicate the spectra of the third control cell with no biostimulants. To better visualize the data and their evolution in time they are represented all together in the graph on top of the figure while measurements referred to different DULs are depicted separately below.

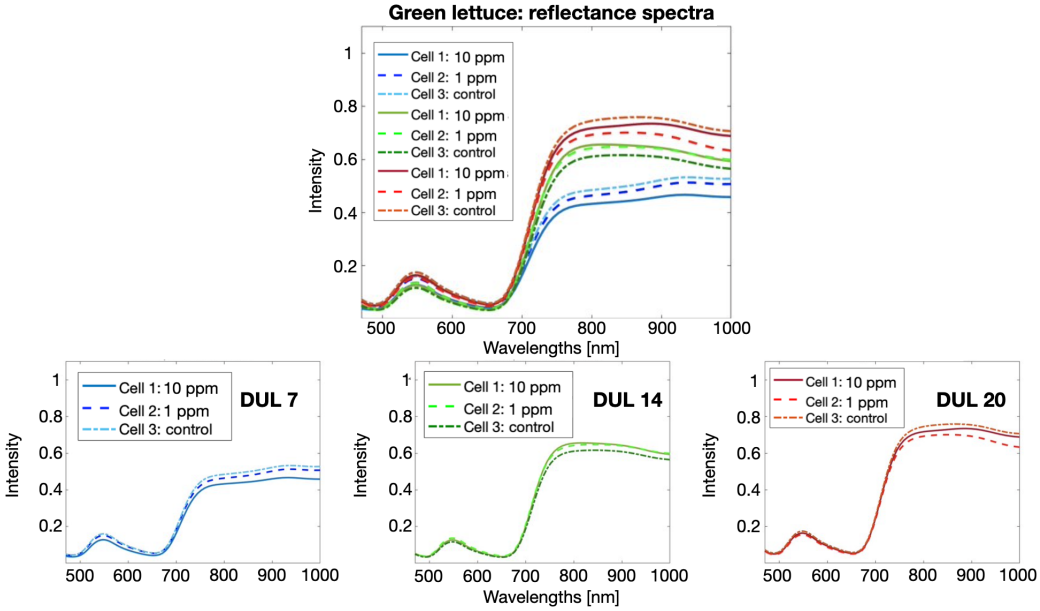

Figure 5.20: Reflectance spectra of the Green lettuce species.

From visual inspection of the spectra referred to the same day, it is possible to note that no obvious difference due to the presence of biostimulants is shown. Differently, when observing the whole temporal evolution of the data, spectral features which characterize the growth of the plants are noticeable. All the samples indeed, biostimulated or not, show an increase of reflectance intensity in the NIR region, particularly between 750 and

950 nm. It is worth noticing that the spectra shown in Figure 5.20 have been obtained mediating over a very big number of leaves, meaning that they significantly represent the overall effect of growth and biostimulants on the species. This was obtained by exploiting the SAM algorithm on the hyperspectral cube (Chapter 3). The spectrum of a manually selected leaf inside the analyzed image was employed as a reference. The result of the application of this algorithm allows a fast selection of the significant pixels in the image, excluding for example the ones referred to soil or background as shown in Figure 5.21.

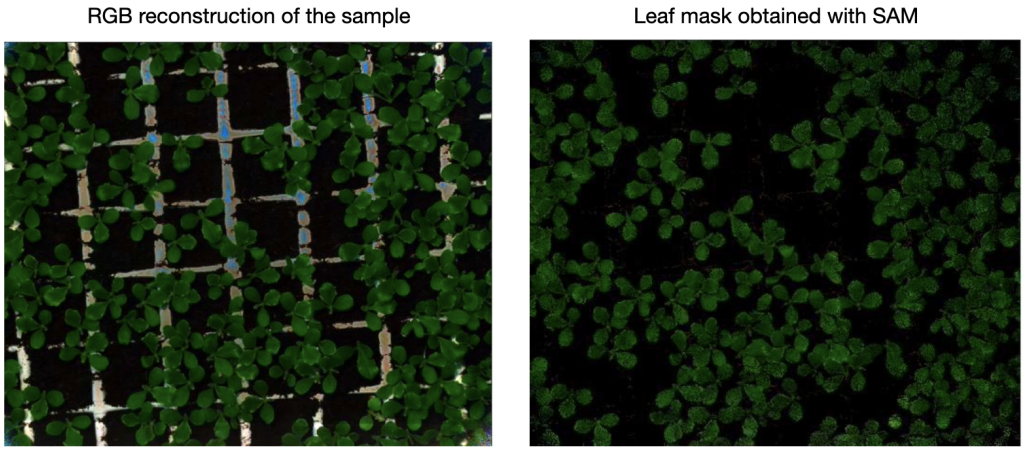

Figure 5.21: Extraction of the significant pixels with the SAM algorithm.

The spectra referred to the other two species under analysis, the Romaine lettuce and Tatsoi species, are reported in Figure 5.22 and 5.23 respectively. Similarly to the Green lettuce species it is not trivial to detect the effect of biostimulants on the spectra of the samples under consideration. We are only able to distinguish changes in a species' spectra over time which are most likely due to its growth: the increased reflectance in the near infrared and the decrease of the peak in the green spectral region that indicates a darkening in the plant's hue (confirmed by visual inspection of the samples). These trends seem common to all the species and all the samples, both stimulated and not.

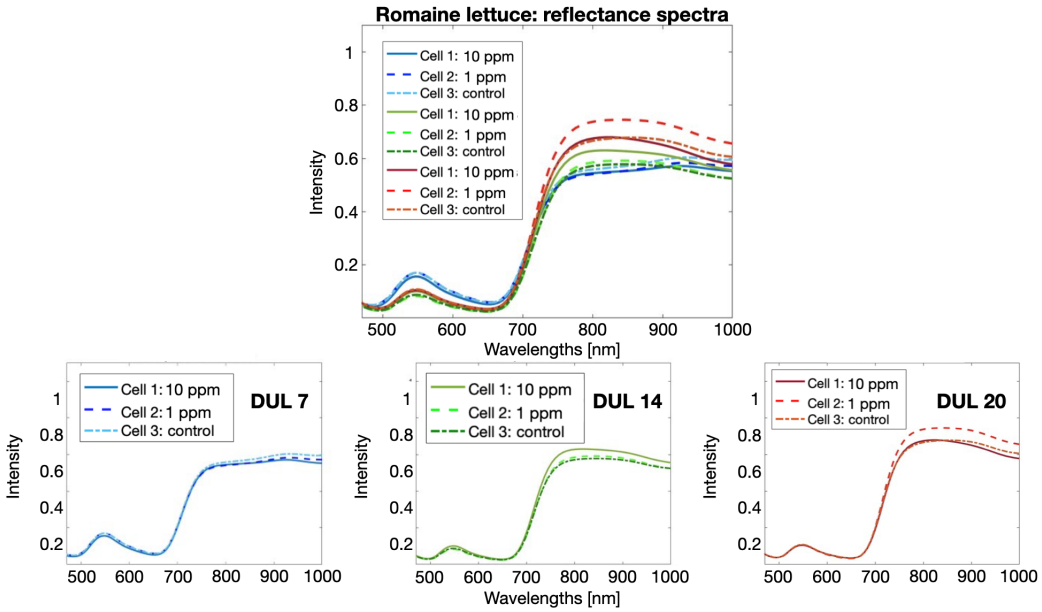

Figure 5.22: Reflectance spectra of the Romaine lettuce species.

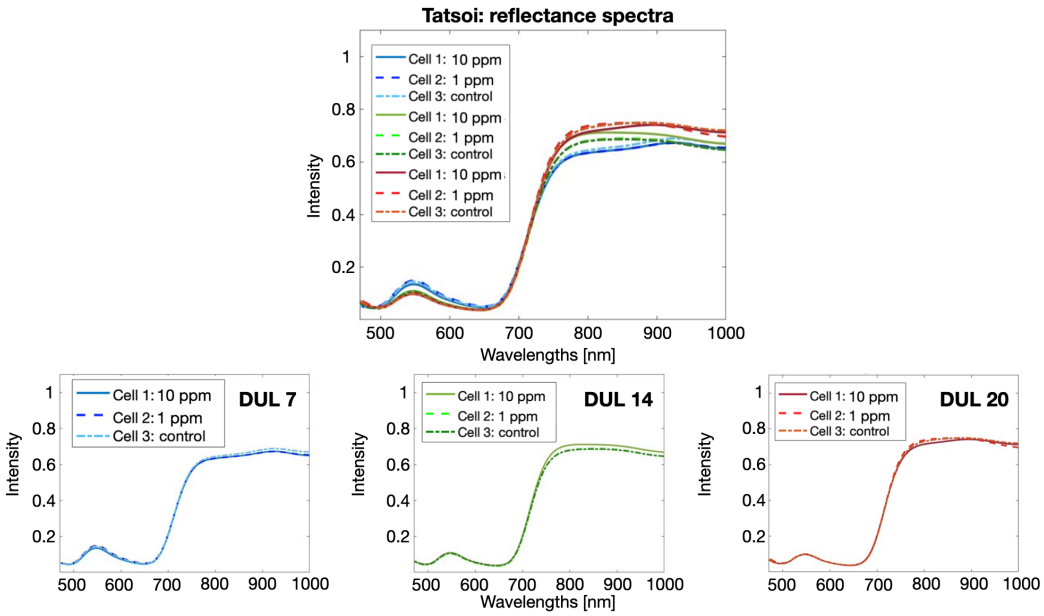

Figure 5.23: Reflectance spectra of the Tatsoi species.

In order to carry out a more detailed analysis and detect the effects of the biostimulants on the growth of the plants, some indices related to relevant spectral features have been computed and their trend over time was plotted. In Figure 5.24 the behaviour of the

mean value of the reflectance spectrum in the NIR region is plotted over the whole measurement campaign for each sample. From the previous analysis of the spectra indeed, we expected this value to increase due to the growth of the leaves and our prediction is confirmed.

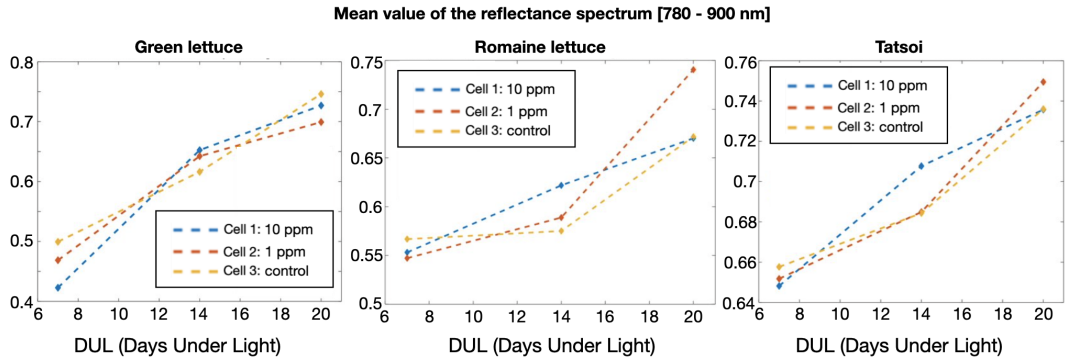

Figure 5.24: Mean value of the value of the reflectance spectrum in the NIR for the 3 species analyzed.

It is interesting to note that the blue line, referred to the cell with the highest value of biostimulants' concentration has the steepest slope in the time interval between DUL 7 and 14. Its increase is instead lower between DUL 14 and 20. When the data were first analyzed this result seemed contradictory with the behaviour shown by the samples of cell 2, where the biostimulants are lower, since the slope of the these data remains higher than the control one for all the measurements (at least in the Romaine lettuce and Tatsoi species). However later in the work it was found that on DUL 16 due to the fact that the leaves experienced an excessive elongation in the first cell, the biostimulants' concentration for these samples was brought to zero, therefore their effect is no longer visible in the growth of the samples. This observation shows that some effect of the biostimulants on the sample's growth is actually present. It also demonstrates that these changes are detectable also in the spectral behaviour of the leaves.
Later the NIR index developed in the study presented in the previous section was plotted, in order to investigate whether the biostimulant's effect would be visible in the behaviour of this index, related to water absorption. Figure 5.25 shows the results of the calculations for the NIR index. Once again it is difficult to detect clear signs of the effect of the biostimulants on the samples. A hint of their magnifying effect plants' growth might be given by the higher slopes of the curves related to biostimulated leaves. However, it is interesting to note that the behaviour of the species is similar in both the indices, indicating that the growth process is very similar for the analyzed plants.
Finally, in order to simplify the problem, the PCA algorithm was employed as introduced in Chapter 3. The principal components have been calculated over the whole

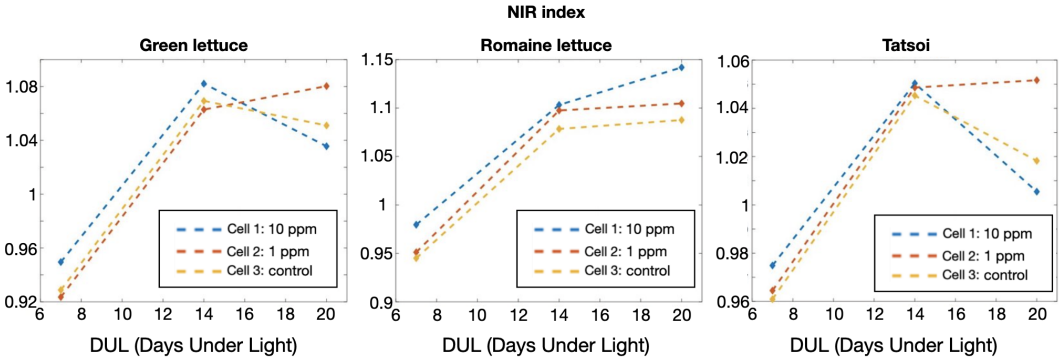

Figure 5.25: NIR index behaviour for biostimulated and control samples.

dataset referring to a single species. This was necessary in order to obtain the principal components maximizing the variance between different measurements. The weights of the first 5 principal components are reported in Figure 5.26.

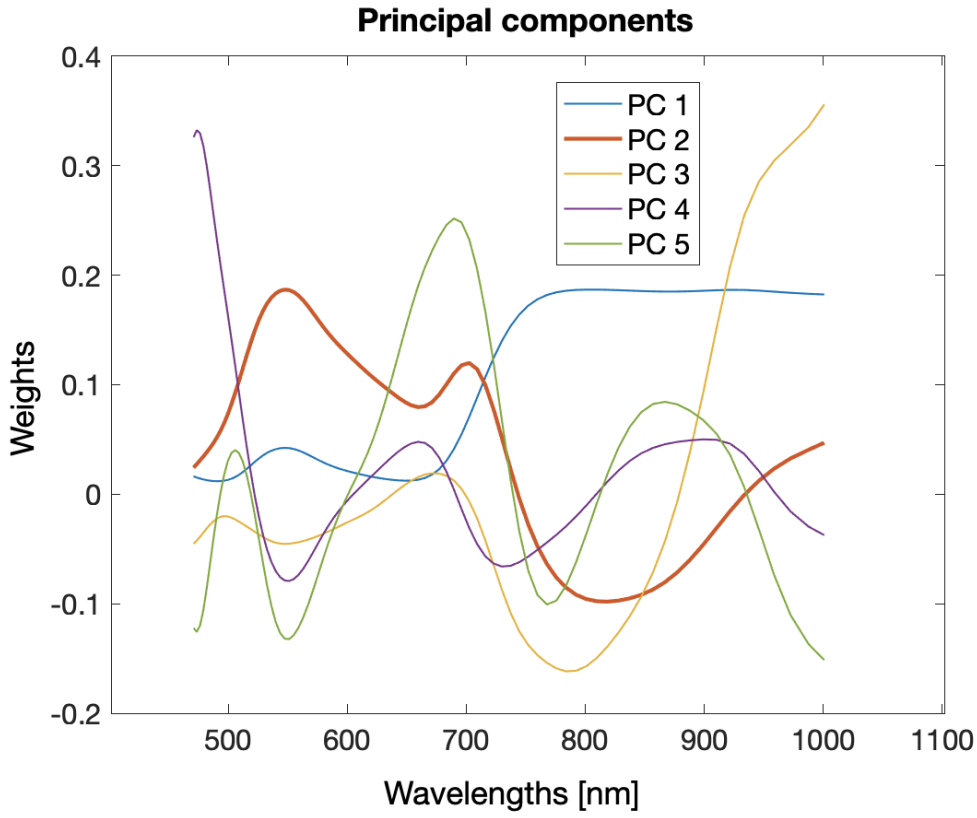

Figure 5.26: Weights of the first 5 principal components for the biostimulated samples.

Among them PC2 was selected as new coordinate to represent the measurements over time. This choice is motivated by the fact that PC1 in this kind of measurement give information on the illumination of the sample, therefore the second principal component will be the one retaining the highest variance related to other features in the image. For doing so, the value of the second principal component has been calculated for all the pixels in each image. In Figure 5.27 measurements are represented as the average PC2 value of the hyperspectral image. This value was calculated over the pixels belonging to the leaves only, exploiting the SAM algorithm.

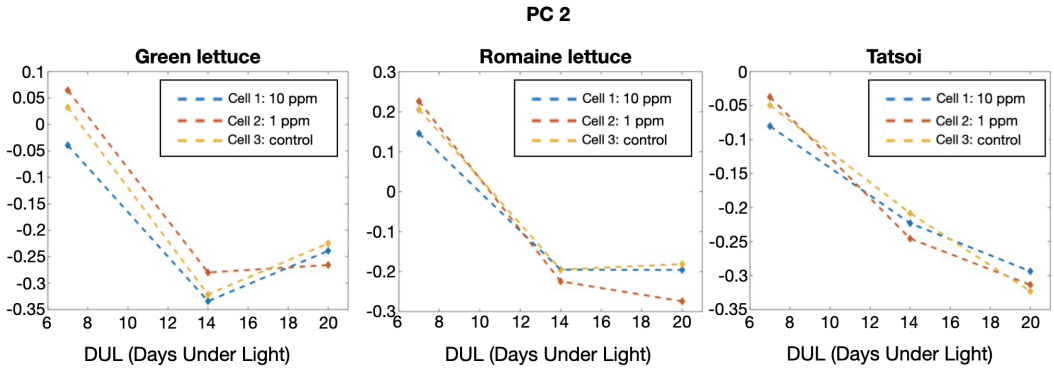

Figure 5.27: PC2 average value for the biostimulated and control samples.

What is most noticeable from the previous figure is the overall decreasing trend, common to all the species both biostimulated and not. By looking at Figure 5.26 it is possible to observe that the weight of the NIR region in the second PC is negative. This behaviour therefore suggests either an increase over time of the reflectance intensity in the Near Infrared or a decrease of reflectance in the visible region. This evolution of the spectra corresponds to what was initially observed through visual inspection of the samples' spectra. PCA analysis therefore confirms the fact that the most important differences in the spectra of the samples analyzed are due to the growth process, while the effects of biostimulants are not clearly distinguishable.

Unfortunately, from this initial hyperspectral analysis is very difficult to detect specific spectral features that indicate the effect of biostimulants. This might be due to the fact that the amount introduced in the plants was not enough to cause significant changes in the concentration of nutrients inside the plant but rather it acted more on their appeareance. The stimulated samples indeed at the end of the study resulted heavier and with larger leaves compared to the others. On the other hand, from the investigation of indices related to the growth of the plant, such as the one related to the NIR reflectance, it is noticeable that their increase is faster, indicating that the biostimulants have a magnifying effect on the growth of the samples. More detailed analysis, possibly employing

finer techniques to distinguish differences in the spectra could be done to further analyze whether the effect of biostimulants is fundamental in the growth of leafy vegetables.

5.2.2 Biostimulants' effect on shelf life

From the same cells employed in the experiment on the effect of biostimulants on the growth of leafy vegetables, samples of the Romaine lettuce and Tatsoi species have been selected to investigate the effect of these biostimulants on their shelf life. In order to guarantee the best preservation of the samples, based on the result of the previous study, the leaves were stored in a sealed plastic box which was placed in a refrigerator at $+4°C$. Measurements were taken on the 5^{th}, 12^{th} and $19th$ day post harvest for both the species. Following the same SAM algorithm employed in the previous part of the study, the mean spectra for all the leaves in the box was calculated and the results are show in Figure 5.28 and 5.29 for the Romaine lettuce and Tatsoi species respectively:

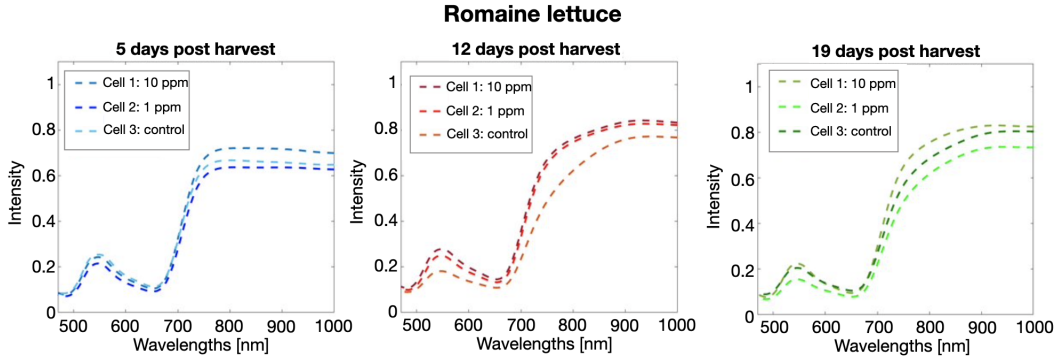

Figure 5.28: Reflectance spectra on the 5^{th}, 12^{th} and $19th$ day post harvest for Romaine lettuce species.

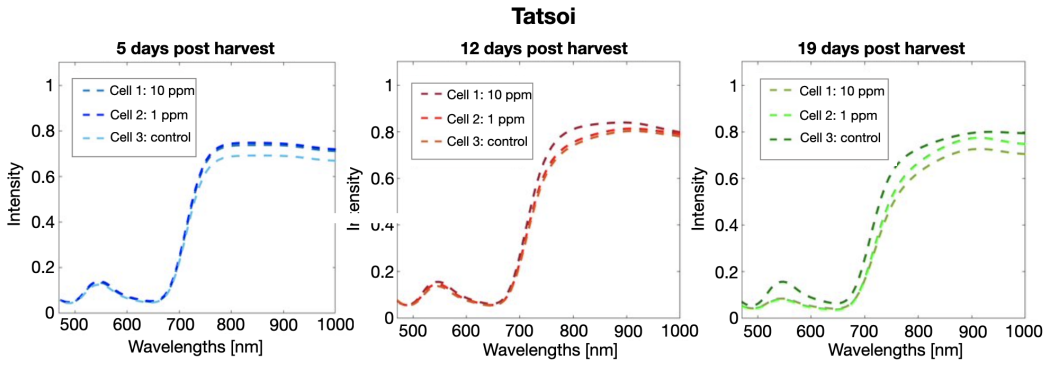

Figure 5.29: Reflectance spectra on the 5^{th}, 12^{th} and $19th$ day post harvest for Tatsoi species.

Similarly to what happened in the first part of the present study, from visual inspection of the spectra, the effect of the biostimulants is not clear. On the other hand, a very interesting spectral feature most likely related to senescence is clearly visible: a decrease in the reflectance intensity in the NIR region around 750 - 800 nm. In order to detect the effect of the stimulating substances on the degradation of the leaves, some known indices which can be related to the senescence of the leaf, presented already in Chapter 3 have been calculated. For example the REP (Red Edge Position) indicates the wavelength at which clorophyll becomes transparent, leading to the high slope between the end of the visible region and the beginning of the NIR in reflectance spectra. Generally the REP is located around 700 nm and an increase in its value indicates senescence in the leaf. The

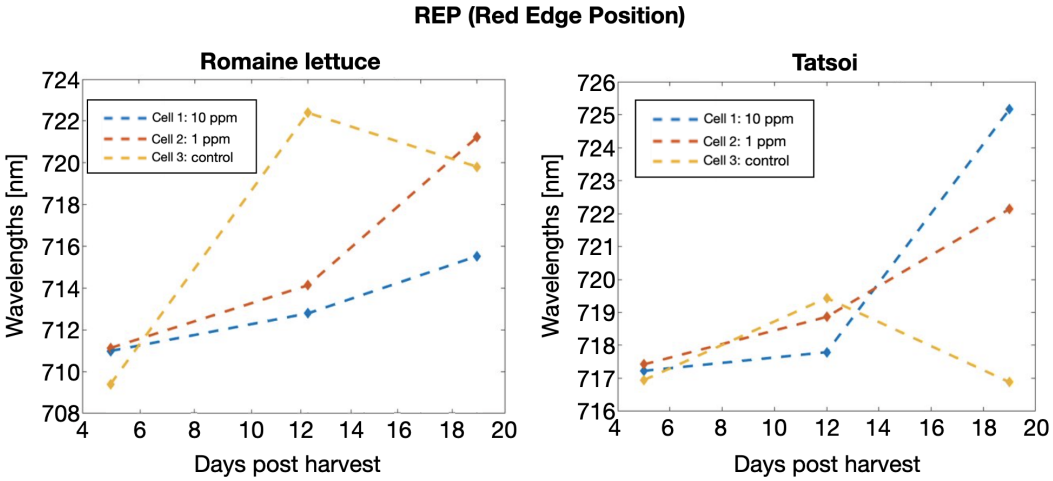

Figure 5.30: Evolution of the Red Edge Position over time for the biostimulated and control species.

representation of the behaviour of this index for the analyzed samples is represented in Figure 5.30.Both the species show a similar behaviour of the blue and red data referring to samples grown in the first and second cell. This similarity can therefore be linked to the effect of biostimulants since their trend differs completely from the behaviour of the data related to the control. Moreover, the stimulated samples experience an increase in the REP as expected.
A second index that has been employed in order to recognize the difference in the senescence process between the samples is the CUR index. Even if the curvature index is not directly related to the degradation of the plant, in a study carried out by Jia et al. [34] it resulted effective in predicting a parameter that is connected to the photosynthetic properties of the plant: the Fv/Fm. Its value is the most used chlorophyll fluorescence measuring parameter, comparing the difference of the minimum fluorescence of the plant with its maximum fluorescence. In general leaf stress is linked to a decrease in the Fv/Fm parameter. The CUR index was found to adequately estimate the value of Fv/Fm through the following equation:

$$\frac{Fv}{Fm} = -0.3963 * CUR + 1.196 \tag{5.3}$$

Estimations of the Fv/Fm value through the CUR index are shown in Figure 5.31:

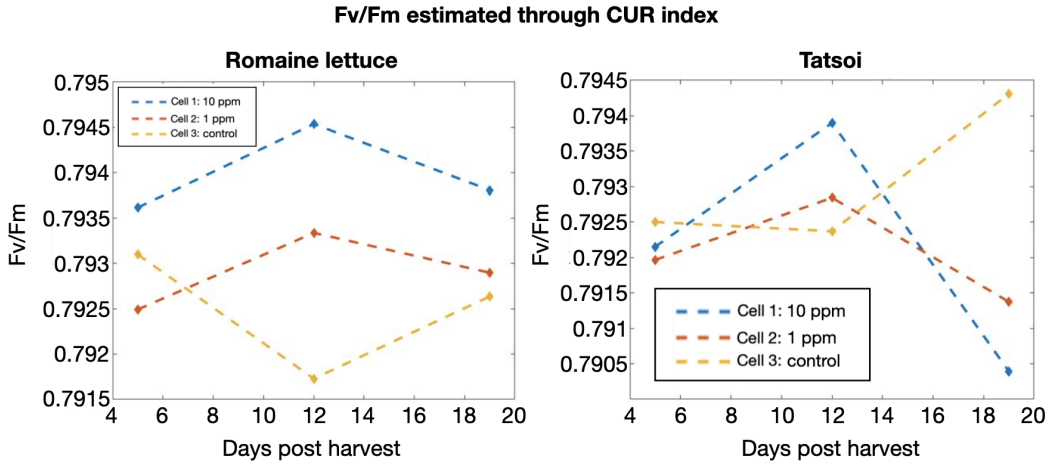

Figure 5.31: Estimation of the value of Fv/Fm through the CUR index for the biostimulated and control species.

Very interestingly it is noticeable again that both the species show a particular behaviour in the biostimulated samples while the non-stimulated ones show a different behaviour, again common to both the species under consideration.

This study, focused on the biostimulants' effects on leafy vegetables, testifies the difficulties in analyzing hyperspectral data. It is clear that the spectra obtained with the hyperspectal measures provide many information and, most importantly, that they are able to reflect very fine differences in samples which are very similar. However, as this study demonstrated, it is not always easy to detect the differences in spectral signatures. More refined mathematical tool can help in the detection of the variations in the spectra but still it might be difficult to link these features to physical or chemical characteristics of the specimen. It was shown for example that the effect of biostimulants is reflected in the behaviour of some indices related to the spectra of the plants, however we're not able to link that particular behaviour to a physical or chemical process happening in the plants. Further studies focused on the biological processes happening in biostimulated growth of plants could help in selecting the spectral regions that are subjected to the most significant changes.

Chapter 6

Conclusions

The analysis presented in this work shows that the HERA Iperpettrale is able to reproduce with fine spectral and spatial resolution the spectral signaturs of leafy vegetables. It is able to distinguishing not only the differences in the spectra between different species of vegetables but also between leaves of the same species and even among different parts of the leaf. This result clearly proofs the great possibilities of hyperspectral imaging in the food and agriculture sector. In the first study on leafy vegetables' shelf life, it was shown that the conservation method greatly influences the senescence process of the leaves. Different degradation paths caused different evolution of the spectra of the plants. The overall picture therefore is more complicated than the one represented at the beginning in Figure 4.4, found in a reference study from Simko et al. [3], depicting a single senescence process. Interestingly, this degradation path is actually very similar to the one experienced by the samples in the second study.
It was shown that the analysis of the VIS region correctly depicts the change of hue of the leaves throughout their lifecycle and that the evolution of the spectral features in this region are able to predict these color shifts even before they are visible by the human eye. The NIR region, instead, resulted fundamental in the first experiments in the distinction between different senescence processes and in particular on their effect in the water content of the leaves. In the spectral range of the HERA Iperspettrale falls indeed the characteristic absorption peak of water around 970 nm. In order to evaluate the strength of this absorption, related to the hydration state of the leaf, the NIR index has been developed. Similarly to the ones found in literature, it links the reflectance intensity with a physical feature of the sample. This index resulted very effective in the prediction of the behaviour of the samples and its trend correctly depicted whether the leaves were undergoing a dehydration process or not.
The first project was also successful in extracting information on the nutrients contained in the leaves both with reflectance and fluorescence data. The fluorescence spectrum of

the leaves indeed was always characterized by two peaks: a bigger one around 750 nm, connected to chlorophylls concentration, and a smaller one, related to the presence of phenolic compounds, around 550 nm. While a decrease in the concentration of chlorophylls has been found as a sign of degradation of the plant, its phenols production does not seem directly linked to senescence. Also in this case, the calculation of an index starting from the intensities of the reflectance spectrum was very useful. The development of the Chlorophyll index indeed was able to confirm the decrease of the concentration of this nutrient in degrading leaves.
In the first study, similarities and differences among spectra were distinguishable by visual inspection since senescence produces macro-changes in the samples. It was therefore easier to decide in which spectral region further analysis had to be implemented in order to better visualize and quantify the differences among spectra due to degradation processes. In the second project, instead, the effect of biostimulants was found to modify only slightly the spectral signature of the samples under analysis. It was shown, therefore, that even if the hyperspectral images provide very reliable and numerous information, it is not always easy to manipulate the hyperspectral cube in order to obtain easily interpretable data. Even if the differences due to biostimulants were not clearly distinguishable, very interestingly instead the effect of growth and degradation on the spectra of the samples were highly visible, similarly to the previous case study. In order to understand whether the effect of stimulating substances influenced the growth or senescence of the plants, well-known indices related to the wellness of the plant have been plotted from the measured spectra. Interestingly, the behaviour of the biostimulated plants was found to be similar in the evolution of the indices and differed from the one of the control. In addition to this the presence of biostimulants seemed to magnify the increase of values characterizing the growth of the plants. These results suggest that the biostimulants do affect the lyfecycle of leafy vegetables, however not in a striking way. The use of algorithms such as the Spectral Angle Mapper were fundamental in this experiment, enabling us to distinguish the relevant parts of the hyperspectral image and perform faster and more significant calculations.

6.1 Further developments

The overall good results obtained in the present work encourage further projects and experiments involving the application of the HERA Iperspettrale in the food and agriculture field. First of all, the importance of the numerical methods for the analysis of the hyperspectral cube resulted clear from the analyzed studies. The use of finer algorithms, implying for example machine learning techniques, would enable to detect smaller differences in the spectra which are not distinguishable by visual inspection. These methods would be able to provide more quantitative results in experiments or perform clustering

to distinguish healthy from ill samples. In order to train the aforementioned algorithms some preliminary studies should be performed to provide reference spectra of healthy plants and characteristic spectra of specific illnesses to be identified.

The results of this work made also clear the importance of the Near Infrared spectral region in the considered applications. Literature research also confirms that many interesting molecules that characterize both the wellness and the nutritional value of vegetables and food more in general, have their characteristic absorption peaks in the SWIR (Short-Wave Infrared) region, up to 2.5 μm [39]. A further improvement of the present thesis would be therefore to examine more in depth the spectral signature of molecules detectable in the SWIR such as glucose and water [40]. A preview of a similar study is presented hereafter. A prototype of a model of the HERA with an infrared detector has been employed over a sample of degraded lettuce, which was kept in the fridge for about 20 days in a sealed plastic box. Some of the leaves resulted very moist and degraded, in Figure 6.1 the spectra of two point of the leaf highlighted in the image are compared.

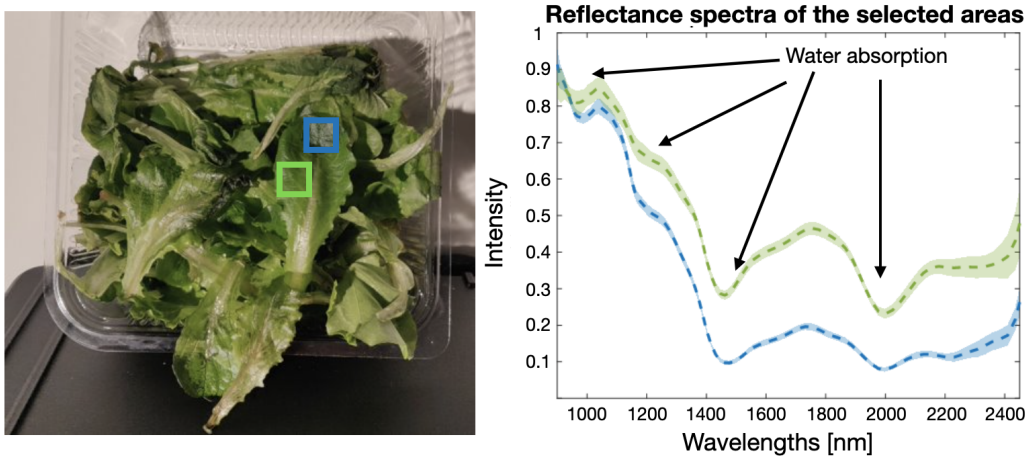

Figure 6.1: Reflectance spectra of the highlighted areas in the picture.

All the four known absorbance peaks of water (already presented in Figure 5.6) are clearly visible in the reflectance spectra. The one referred to the blue area are more pronounced, suggesting that the corresponding area of the leaf has a higher water content. This hypothesis is actually confirmed both by visual inspection and by performing a reconstruction of the image in correspondence of an absorption window (Figure 6.2). By plotting the relative intensity of the reflectance at 1450 nm, where a peak is located, a differently shaded area is recognizable in the analyzed leaf. This means that the relative component has a weaker intensity in that area and the light at this wavelength is more

strongly absorbed.

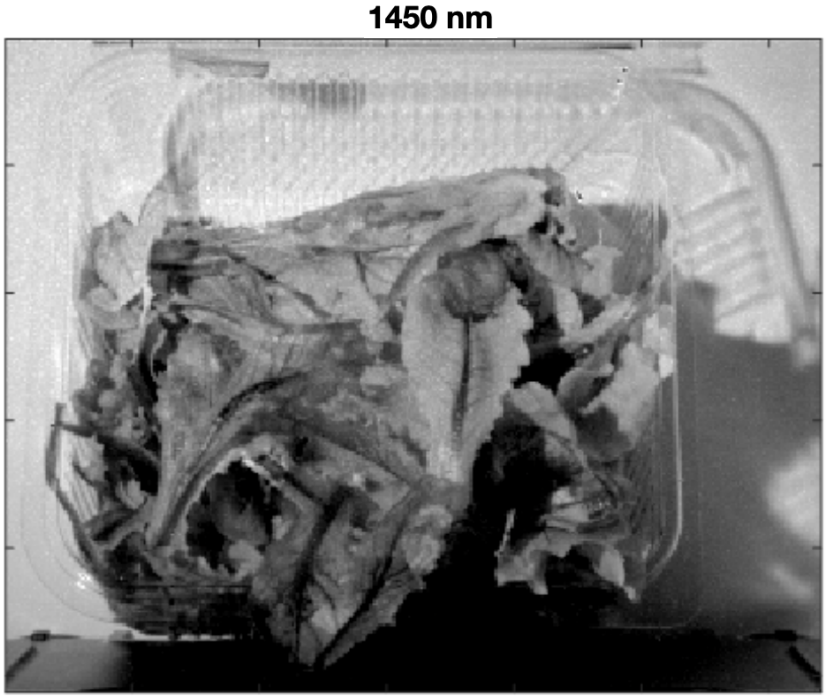

Figure 6.2: Reconstruction of the image at 1450 nm, corresponding to a water absorption peak.

The potentialities of the examination of this spectral range are therefore already clear from this preliminary example.

Regarding the more industrial-related application of this study, starting from hyperspectral studies it would be possible to develop quality-checking systems specifically designed for plants. Indeed, by selecting the most important spectral bands to monitor the wellness and growth of the products, such as the ones related to chlorophylls or the hydration status, a simpler multi-spectral system could be designed. Multi-spectral imaging, as explained in Chapter 2, retrieves the intensity of the spectra related to a smaller number of bands, therefore is easier and cheaper to implement technologically a multi-spectral camera.

As a final remark, further studies in close collaboration with experts in biology and agriculture would enable a better understanding of the physicochemical properties that underlie the spectral behaviours. Knowing which molecules or processes guide the growth

and senescence of plants, would indeed help the selection of relevant spectral regions to be monitored in the search for a particular behaviour. This awareness would enable a more specific and detailed analysis, together with the use of more refined algorithms and indices.

Appendix A

MATLAB code

In the following section the MATLAB code employed for the calculation of the spectrum of an area the sample is presented. Later on, the SAM algorithm and the PCA algorithm performed as explained in Chapter 3 are reported in MATLAB code.

```
%% Spectrum of an area of the sample for different
   images

% loading of the files
file_name = {'file_1.mat','file_2.mat','file_3.mat'};

color = {'#0072BD';'#77AC30';'#D95319';...
         '#EDB120';'#7E2F8E';'#4DBEEE';'#A2142F'};
p = {[0 0.4470 0.7410],[0.4660 0.6740 0.1880],...
     [0.8500 0.3250 0.0980],[0.9290 0.6940 0.1250],...
     [0.4940 0.1840 0.5560],[0.3010 0.7450 0.9330]};

%select wheter the measures are in reflectance
refl = 1;

load('file_1_WavelengthAxis')

wl = HERA_WavelengthAxis;

for i = 1:length(file_name)

    load(file_name{i})
```

```
22      hypdata = HERA_HSI;
23
24      %reconstruct the RGB image from the hyperspectral
            data
25
26      RGB_image = RGB_reconstruction(hypdata,wl,refl);
27
28      %calculate the average spectrum of a selected area
29      spectrum_area = AreaSpectrum(RGB_image,hypdata,wl,
            ...
30      color{i},p{i});
31
32  end
33
34  function RGB_image = RGB_reconstruction(hyp,wl,refl)
35      %find the indices in the wavelength array
            corresponding
36      to the RGB values
37
38      [~,lambda1] = min(abs(wl - 630)) ; %R
39      [~,lambda2] = min(abs(wl - 540));  %G
40      [~,lambda3] = min(abs(wl - 500));  %B
41
42      %Select the portions of the hyperspectral cube
43      if refl == 1
44
45          band_1 = hyp(:,:,lambda1);
46          band_2 = hyp(:,:,lambda2);
47          band_3 = hyp(:,:,lambda3);
48      else
49      % normalize if the data is not in reflectance
50          band_1 = hyp(:,:,lambda1)/max(max(hyp(:,:,
                lambda1)));
51          band_2 = hyp(:,:,lambda2)/max(max(hyp(:,:,
                lambda2)));
52          band_3 = hyp(:,:,lambda3)/max(max(hyp(:,:,
                lambda3)));
```

```
53      end
54
55      RGB_image = cat(3,band_1, band_2,band_3);
56
57  end
58
59
60  function spectrum_area = AreaSpectrum(image,hyp,w,c1,c2)
61
62      %cut the area of the image to obtain the
63      data cube referring to it only
64
65      data_cut = cut_area(image,hyp,c1,c2);
66
67      [rows,columns,bands] = size(data_cut);
68
69      %reshape the hyperspectral cube as a matrix = pixels
            x bands
70      the rows of the matrix constitute the spectrum of
           the pixel
71
72      data_resh = reshape(data_cut,rows*columns,bands);
73
74      [i,j,k] = size(data_cut);
75      X = reshape(abs(data_cut),i*j,k);
76
77      % calculate the mean of the spectra over the
           selected area
78      spectrum_area = mean(X,1);
79      %calculate the standard deviation
80      sd = std(X);
81      sd1 = spectrum_area + 0.5*sd;
82      sd2 = spectrum_area - 0.5*sd;
83
84      figure (2)
85      plot(w,squeeze(abs(spectrum_area)),'Color',...
86      c1,'LineStyle','--','LineWidth',2)
```

```
87      title('Spectra of the selected areas');
88      xlabel('Wavelengths [nm]')
89      ylabel('Intensity')
90      hold on
91
92      p = patch([w fliplr(w)],[sd1 fliplr(sd2)],c2);
93     set(p,'facealpha',0.3);
94     set(p, 'EdgeColor', 'None');
95     axis([470 1000 0 1.1])
96     hold on
97
98  end
99
100 %% PCA
101
102 %Perform the matrix factorization shown in Chapter 3
103
104 [m,n,k] = size(hypdata);
105
106 X = reshape(abs(hypdata),m*n,k);
107
108
109 X(isinf(X)|isnan(X)) = 0;
110 [coeff,~,variances] = pca(X(:,1:93));
111
112    %calculate the PCA matrix
113     pca_matrix = X(:,1:93)*coeff;
114
115     %retrieve the PC values of the image
116     pca_1 = reshape(pca_matrix(:,1),m,n);
117     pca_2 = reshape(pca_matrix(:,2),m,n);
118     pca_3 = reshape(pca_matrix(:,3),m,n);
119     pca_4 = reshape(pca_matrix(:,4),m,n);
120     pca_5 = reshape(pca_matrix(:,5),m,n);
121
122     figure
123     imagesc(pca_1)
```

```
    title('PC 1')
    colormap('gray')


% coefficients for the principal components
figure
plot(wl(1:93), coeff(:,1),'LineStyle','-','LineWidth',2)
hold on
plot(wl(1:93), coeff(:,2),'LineStyle','-','LineWidth',2)
hold on
plot(wl(1:93), coeff(:,3),'LineStyle','-','LineWidth',2)
hold on
plot(wl(1:93), coeff(:,4),'LineStyle','-','LineWidth',2)
hold on
plot(wl(1:93), coeff(:,5),'LineStyle','-','LineWidth',2)
title('PCA coefficients')

%Plot the variance relative to the principal components
figure
plot(variances/max(variances),'LineStyle','-',...
'LineWidth',2);
xlabel('Principal Component')
ylabel('Variance')

figure
semilogy(variances/max(variances),'LineStyle','-',...
'LineWidth',2)
xlabel('Principal Component')
ylabel('Variance')


%% SAM

% Calculate the reference spectrum
selecting from an area of the image

RGB_image_leaf = RGB_reconstruction(leaf,wl,refl);
```

```
161
162 area_leaf = cut_area(RGB_image_leaf,leaf,'None');
163
164 [i,j,k] = size(area_leaf);
165 X = reshape(abs(area_leaf),i*j,k);
166
167 spectrum_area_leaf = mean(X,1); %reference spectrum of
      the leaf
168
169 %Perform the comparison
170
171 [rows,columns,bands] = size(leaf);
172 leaf_resh = reshape(abs(leaf),rows*columns,bands);
173 num_pixel = rows*columns;
174 leaf_resh = leaf_resh';
175
176
177 leaf_resh(isnan(leaf_resh))=0;
178
179 %calculate the spectral angle with
180 respect to the reference spectrum
181
182 sp_angle_leaf = zeros(1,num_pixel);
183
184     for i = 1:num_pixel
185         sp_angle_leaf(i) = acos((leaf_resh(:,i)'*
              spectrum_area_leaf')/...
186         (norm(leaf_resh(:,i))*norm(spectrum_area_leaf)))
              ;
187     end
188
189 SAM_leaf = abs(reshape(sp_angle_leaf,rows,columns));
190
191 figure
192 histogram(SAM_leaf)
193 title('SAM with reference spectrum')
194 xlabel('Spectral Angle')
```

```
195
196 %select the threshold for the spectral angle
197 threshold = 0.2;
198
199 % compute a mask to show only the pixels
200 in the cluster of the referencec spectrum
201
202 mask_leaf = zeros(1,num_pixel);
203     for i = 1:num_pixel
204         if sp_angle_leaf(i) <= threshold
205             mask_leaf(i) = 1;
206         end
207     end
208
209 mask_leaf = reshape(mask_leaf,rows,columns);
210
211 leaves = leaf.*mask_leaf;
212
213 RGB_leaves = RGB_reconstruction(leaves,wl,refl);
214
215 figure
216 imagesc(RGB_leaves)
217 title('Leaf mask')
```

Bibliography

[1] Miguel Ángel Lara Blas. "Hyperspectral image applied to determine quality parameters in leafy vegetables". 2016.

[2] Miguel Ãngel Lara et al. "Hyperspectral Imaging to Evaluate the Effect of IrrigationWater Salinity in Lettuce". In: *Applied Sciences* 6.12 (2016). ISSN: 2076-3417.

[3] Ivan Simko, Jose A. Jimenez-Berni, and Robert T. Furbank. "Detection of decay in fresh-cut lettuce using hyperspectral imaging and chlorophyll fluorescence imaging". In: *Postharvest Biology and Technology* 106 (2015), pp. 44–52. ISSN: 0925-5214.

[4] Hongyu Huang Tao Zeng Jun Li and Noriyuki Kobayashi. "Visualization of Chlorophyll Change in Spinach by Hyperspectral Imaging". In: *Journal of Chemistry and Chemical Sciences* 8 (2018), pp. 1201–1209.

[5] Fabrizio Preda, Antonio Perri, and Dario Polli. "A New Hera in Hyperspectral Imaging". In: *PhotonicsViews* 18.1 (2021), pp. 45–49.

[6] Hans F. Grahn and Paul Geladi. *Techniques and Applications of Hyperspectral Image Analysis*. John Wiley Sons, Ltd, 2007.

[7] Chao Deng et al. "Snapshot hyperspectral imaging via spectral basis multiplexing in Fourier domain". In: *Optics Express* 26.25 (Nov. 2018), p. 32509. ISSN: 1094-4087.

[8] Nathan A. Hagen et al. "Snapshot advantage: a review of the light collection improvement for parallel high-dimensional measurement systems". In: *Optical Engineering* 51.11 (2012), pp. 1–8. DOI: 10.1117/1.OE.51.11.111702. URL: https://doi.org/10.1117/1.OE.51.11.111702.

[9] James A. de Haseth Peter R. Griffiths. *Fourier Transform Infrared Spectrometry*. John Wiley Sons, Ltd, 2007.

[10] Wikipedia. *Wiener-Khinchin theorem — Wikipedia, The Free Encyclopedia*. 2021. URL: %5Curl%7Bhttps://en.wikipedia.org/wiki/Wiener-Khinchin_theorem#cite_note-C._Chatfield_1989_94-95-1%7D.

[11] T. Hirschfeld. "Fellgett's Advantage in uv-VIS Multiplex Spectroscopy". In: *Appl. Spectrosc.* 30.1 (Jan. 1976), pp. 68–69. URL: http://as.osa.org/abstract.cfm?URI=as-30-1-68.

[12] A. Candeo et al. "A hyperspectral microscope based on an ultrastable common-path interferometer". In: *APL Photonics* 4.12 (2019), p. 120802.

[13] Daniele Brida, Cristian Manzoni, and Giulio Cerullo. "Phase-locked pulses for two-dimensional spectroscopy by a birefringent delay line". In: *Opt. Lett.* 37.15 (Aug. 2012), pp. 3027–3029.

[14] Antonio Perri. "Visible and near-infrared Fourier transform spectroscopy with a common-path interferometer". In: *Journal of Physics B: Atomic, Molecular and Optical Physics* 54.11 (June 2021), p. 113001. DOI: 10.1088/1361-6455/ac02d1. URL: https://doi.org/10.1088/1361-6455/ac02d1.

[15] A. Perri et al. "Hyperspectral imaging with a TWINS birefringent interferometer". In: *Opt. Express* 27.11 (May 2019), pp. 15956–15967.

[16] Joseph R. Lakowicz. *Principles of Fluorescence Spectroscopy*. Springer Science Business Medi, 2013.

[17] Joliffe I.T. *Principal Component Analysis,Second Edition*. Springer, 2002.

[18] Venkat Rashmi S. Swapna Addamani and Ravikiran S. "Spectral Angle Mapper Algorithm for Remote Sensing Image Classification". In: *IJISET - International Journal of Innovative Science, Engineering Technology* 1.4 (2014).

[19] Marcello Picollo et al. "Hyper-Spectral Imaging Technique in the Cultural Heritage Field: New Possible Scenarios". In: *Sensors* 20.10 (2020).

[20] Claudia Pelosi et al. "Beyond the visible: The Viterbo Crucifixion panel painting attributed to Michelangelo Buonarroti". In: *Microchemical Journal* 154 (2020), p. 104636.

[21] Stefano Laureti et al. "Development of integrated innovative techniques for paintings examination: The case studies of The Resurrection of Christ attributed to Andrea Mantegna and the Crucifixion of Viterbo attributed to Michelangelo's workshop". In: *Journal of Cultural Heritage* 40 (May 2019). DOI: 10.1016/j.culher.2019.05.005.

[22] Mary B. Stuart, Andrew J. S. McGonigle, and Jon R. Willmott. “Hyperspectral Imaging in Environmental Monitoring: A Review of Recent Developments and Technological Advances in Compact Field Deployable Systems”. In: *Sensors* 19.14 (2019).

[23] William R. Johnson et al. “Snapshot hyperspectral imaging in ophthalmology”. In: *Journal of Biomedical Optics* 12.1 (2007), pp. 1–7. DOI: 10.1117/1.2434950. URL: https://doi.org/10.1117/1.2434950.

[24] Guolan Lu and Baowei Fei. “Medical hyperspectral imaging: a review”. In: *Journal of Biomedical Optics* 19.1 (2014), pp. 1–24.

[25] Raúl Siche et al. “Evaluation of food quality and safety with hyperspectral imaging (HSI)”. In: *Food Engineering Reviews* 8.3 (2016), pp. 306–322.

[26] Julio Nogales-Bueno et al. “Determination of technological maturity of grapes and total phenolic compounds of grape skins in red and white cultivars during ripening by near infrared hyperspectral image: A preliminary approach”. In: *Food Chemistry* 152 (2014), pp. 586–591.

[27] Hoonsoo Lee et al. “Detection of Cracks on Tomatoes Using a Hyperspectral Near-Infrared Reflectance Imaging System”. In: *Sensors* 14.10 (2014), pp. 18837–18850.

[28] Xiaolin Zhu and Guanghui Li. “Rapid detection and visualization of slight bruise on apples using hyperspectral imaging”. In: *International Journal of Food Properties* 22.1 (2019), pp. 1709–1719.

[29] Patrick M Mehl et al. “Development of hyperspectral imaging technique for the detection of apple surface defects and contaminations”. In: *Journal of Food Engineering* 61.1 (2004), pp. 67–81. ISSN: 0260-8774.

[30] Gamal ElMasry, Ning Wang, and ClÃ©ment Vigneault. “Detecting chilling injury in Red Delicious apple using hyperspectral imaging and neural networks”. In: *Postharvest Biology and Technology* 52.1 (2009), pp. 1–8. ISSN: 0925-5214.

[31] Santosh Lohumi et al. “Application of hyperspectral imaging for characterization of intramuscular fat distribution in beef”. In: *Infrared Physics Technology* 74 (2016), pp. 1–10. ISSN: 1350-4495.

[32] Wei Zhang et al. “Non-destructive internal quality assessment of eggs using a synthesis of hyperspectral imaging and multivariate analysis”. In: *Journal of Food Engineering* 157 (2015), pp. 41–48.

[33] Anatoly A et al. Gitelson. "Nondestructive estimation of anthocyanins and chlorophylls in anthocyanic leaves". In: *American journal of botany* 96 (2009).

[34] Min Jia et al. "Quantifying Chlorophyll Fluorescence Parameters from Hyperspectral Reflectance at the Leaf Scale under Various Nitrogen Treatment Regimes in Winter Wheat". In: *Remote Sensing* 11.23 (2019).

[35] Andrés Viña and Anatoly A. Gitelson. "Sensitivity to Foliar Anthocyanin Content of Vegetation Indices Using Green Reflectance". In: *IEEE Geoscience and Remote Sensing Letters* 8.3 (2011), pp. 464–468.

[36] Baofeng Su Jinru Xue. "Significant Remote Sensing Vegetation Indices: A Review of Developments and Applications". In: *Journal of Sensors* 2017 (2017).

[37] Kent F. Palmer and Dudley Williams. "Optical properties of water in the near infrared∗". In: *J. Opt. Soc. Am.* 64.8 (Aug. 1974), pp. 1107–1110. DOI: 10.1364/JOSA.64.001107. URL: http://www.osapublishing.org/abstract.cfm?URI=josa-64-8-1107.

[38] M. Saleem et al. "Laser-induced fluorescence spectroscopy for early disease detection in grapefruit plants". In: *Photochem. Photobiol. Sci.* 19 (5 2020), pp. 713–721. DOI: 10.1039/C9PP00368A. URL: http://dx.doi.org/10.1039/C9PP00368A.

[39] David Kim et al. "Highly sensitive image-derived indices of water-stressed plants using hyperspectral imaging in SWIR and histogram analysis". In: *Scientific Reports* 5 (Nov. 2015), p. 15919. DOI: 10.1038/srep15919.

[40] David Kim et al. "Highly sensitive image-derived indices of water-stressed plants using hyperspectral imaging in SWIR and histogram analysis". In: *Scientific Reports* 5 (Nov. 2015), p. 15919. DOI: 10.1038/srep15919.